ISSN: 2641-1911
DOI: 10.33552/ANN.2026.18.000936
Archives in Neurology & Neuroscience
Iris Publishers

Review Article

Cerebral Aneurysm Hemodynamics: from Computational Modeling to Clinical Translation

Mohammad Yaghoub Abdollahzadeh Jamalabadi*

Department of Marine Engineering, Chabahar Maritime University, Chabahar, Iran

***Corresponding author:** Mohammad Yaghoub Abdollahzadeh Jama labadi, Department of Marine Engineering, Chabahar Maritime University, Chabahar, Iran.

Received Date: March 06, 2026

Published Date: March 16, 2026

Abstract

Background: Cerebral aneurysms affect 3-5% of the adult population, and their rupture leads to subarachnoid hemorrhage with devastating consequences. Despite established clinical and morphological risk factors, predicting which aneurysms will rupture remains a formidable challenge, driving intense interest in the hemodynamic forces that govern aneurysm behavior.

Objective: This comprehensive review synthesizes three decades of research on cerebral aneurysm hemodynamics, critically examining the evolution of computational fluid dynamics (CFD) methodologies, their validation through advanced imaging, and the translational journey toward clinical implementation.

Methods: We systematically analyze the hemodynamic modeling pipeline-from image acquisition and segmentation to mesh generation, boundary conditions, and numerical solvers-highlighting sources of variability and uncertainty. The review integrates findings from over 170 studies, encompassing epidemiological data, in vitro validation with particle image velocimetry, in vivo validation with 4D Flow MRI, and emerging machine learning applications.

Key Findings: Wall shear stress (WSS) and its derivatives have emerged as central hemodynamic biomarkers, though their relationship with rupture risk is paradoxically bidirectional-both low WSS (promoting inflammatory degeneration) and high WSS (triggering mural weakening) have been implicated. Morphological factors including aspect ratio, location, and daughter blebs interact critically with hemodynamic patterns. While patient-specific CFD provides unprecedented insight into intra-aneurysmal flow, multicenter initiatives reveal substantial variability in WSS quantification, with imaging modality, segmentation technique, and mesh resolution representing major uncertainty sources.

Clinical Implications: Despite compelling retrospective associations, hemodynamic analysis has not achieved routine clinical adoption. Translation requires: (1) standardization of imaging and modeling protocols, (2) prospective multicenter validation, (3) integration with clinical and morphological risk scores, and (4) development of simplified parameters accessible to clinicians.

Future Directions: Emerging technologies including fluid-structure interaction, multiscale modeling incorporating cellular processes, and machine learning-based prediction algorithms promise to enhance predictive capability. Ultra-high-field 7T MRI and accelerated 4D Flow techniques are narrowing the validation gap between simulation and in vivo measurement.

Conclusions: Hemodynamic forces are undeniable determinants of aneurysm pathobiology, yet their clinical utility remains incompletely realized. Bridging the gap between computational sophistication and clinical practicality represents the foremost challenge-and opportunity-for the next decade of aneurysm research.

Keywords: Cerebral aneurysms, Computational fluid dynamics, Wall shear stress, 4D Flow MRI, Rupture risk prediction, Hemodynamics, Patient-specific modeling, Clinical translation

Introduction

Intracranial aneurysms are pathological dilations of cerebral arteries that affect approximately 3-5% of the adult population [114, 159, 161]. While many aneurysms remain asymptomatic throughout life, aneurysm rupture leads to subarachnoid hemorrhage (SAH), a devastating condition associated with high mortality and morbidity rates [67, 100, 113, 154]. The annual incidence of aneurysmal SAH ranges from 6 to 16 per 100,000 population, with case fatality rates approaching 50% in some studies [1, 67, 100]. Figure 1 illustrates the ultrastructure of brain capillaries, highlighting the anatomical basis of the blood-brain barrier (BBB). It emphasizes that the endothelium is non-fenestrated, connected by tight junctions, and lacks Aquaporin-1 (AQP-1) expression. This specific configuration creates a highly selective, non-permeable barrier that meticulously regulates the passage of substances from the bloodstream into the brain's interstitial fluid, a concept fundamental to understanding cerebral physiology and the challenges of drug delivery. The management of unruptured intracranial aneurysms presents a clinical dilemma, as the risks of preventive treatment must be weighed against the natural history risk of rupture. Large prospective studies have established that aneurysm size, location, and patient characteristics influence rupture risk. However, these factors alone cannot fully predict which aneurysms will rupture, leading to increased interest in hemodynamic determinants. Hemodynamic forces, particularly wall shear stress (WSS), have emerged as critical factors in vascular pathophysiology. In cerebral aneurysms, abnormal hemodynamics are implicated in endothelial dysfunction, inflammation, and wall remodeling that may predispose to growth and rupture. Computational fluid dynamics has become the predominant tool for investigating intra-aneurysmal hemodynamics.

The management of unruptured intracranial aneurysms presents a clinical dilemma, as the risks of preventive treatment must be weighed against the natural history risk of rupture [24, 47, 69, 77, 108, 131, 148, 164, 167, 168]. Large prospective studies have established that aneurysm size, location, and patient characteristics influence rupture risk [37, 62, 63, 64, 94, 132, 148]. However, these factors alone cannot fully predict which aneurysms will rupture, leading to increased interest in understanding the hemodynamic environment as a potential determinant of aneurysm behavior [15, 30, 122]. Hemodynamic forces, particularly wall shear stress (WSS), have emerged as critical factors in vascular pathophysiology [87, 92, 122]. In cerebral aneurysms, abnormal hemodynamics are implicated in endothelial dysfunction, inflammation, and wall remodeling that may predispose to growth and rupture [10, 91, 125]. Computational fluid dynamics has become the predominant tool for investigating intra-aneurysmal hemodynamics, offering detailed quantification of velocity fields, WSS distributions, and other flow parameters [13, 122, 144].

Figure 1: brain capillaries, the endothelium lacks fenestrations, contains tight junctions, and suppresses AQP-1 expression, resulting in a non-permeable barrier that strictly regulates substrate entry into the brain interstitial space.

This review aims to provide a comprehensive overview of the current state of knowledge regarding cerebral aneurysm hemodynamics, with specific focus on: [1] CFD methodologies and their evolution, [2] imaging techniques for model construction and validation, [3] hemodynamic parameters associated with rupture risk, [4] the influence of morphological factors, [5] validation studies comparing CFD with in vitro and in vivo measurements, and [6] clinical applications and translational challenges. Figure 2 contrasts the blood-cerebrospinal fluid barrier (BCSFB) located at the choroid plexus with the barrier at the ependymal lining. It shows that while the choroid plexus capillaries are fenestrated to allow fluid filtration, the overlying epithelial cells are sealed by tight junctions, forming the restrictive barrier. In contrast, the ependymal cells that line the ventricles communicate via gap junctions, permitting the free exchange of fluid between the ventricular system and the brain's interstitial space, illustrating the different levels of barrier function within the brain's fluid compartments.

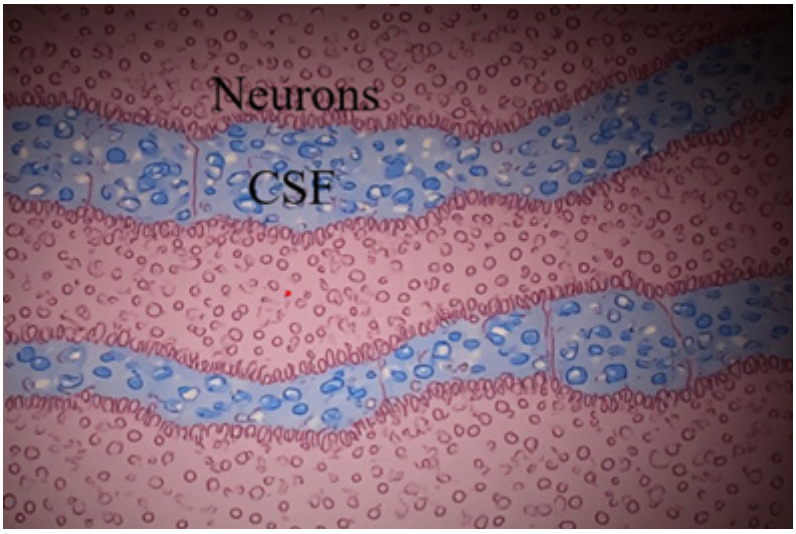

Figure 2: The choroid plexus forms the blood–CSF barrier. Its capillaries are fenestrated, but tight junctions between epithelial cells prevent free passage. In contrast, ependymal cells use gap junctions, allowing CSF to mix freely with interstitial fluid.

Epidemiology and Natural History of Intracranial Aneurysms

Prevalence and Incidence

The prevalence of intracranial aneurysms in the general population has been estimated through systematic reviews and large imaging studies. Rinkel et al. [114] reported a prevalence of approximately 2-3% in adults, while subsequent meta-analyses by Vlak et al. [161] found a slightly higher prevalence of 3.2%, with increased rates in patients with autosomal dominant polycystic kidney disease and those with a family history of aneurysms. The International Study of Unruptured Intracranial Aneurysms (ISUIA) provided comprehensive data on the natural history of both ruptured and unruptured aneurysms [47, 148]. Vernooij et al. [159] examined incidental findings on brain MRI in the general population and identified aneurysms in 1.8% of adults, with higher prevalence in older age groups. Multiple aneurysms occur in approximately 15-30% of patients with intracranial aneurysms [65, 148]. Kaminogo et al. [65] reported that patients with multiple aneurysms had distinct demographic characteristics and outcomes compared to those with single aneurysms. Figure 3 delineates the multi-layered barrier system established by the arachnoid mater, known as the outer brain barrier (OBB). It points out that although capillaries in the overlying dura mater are fenestrated, the specialized arachnoid barrier cells form a protective layer through tight junctions. Furthermore, vessels traversing the subarachnoid space are sealed by their own vascular walls, ensuring that below the pia mater, the cerebrospinal fluid (CSF) can freely communicate with the brain's interstitial fluid, maintaining the brain's unique fluid environment.

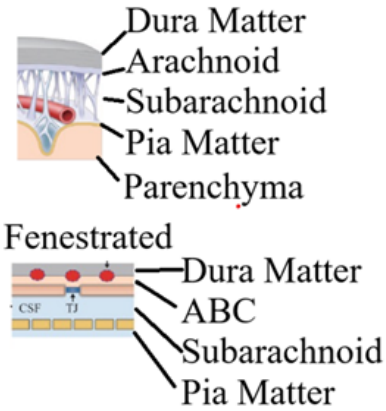

Figure 3: The arachnoid mater establishes the outer brain barrier. While capillaries in the dura mater are fenestrated, tight junctions between arachnoid barrier cells form the outer brain barrier (OBB). Vessels in the subarachnoid space are sealed by their tunica, and capillaries within the barrier have tight endothelium. Below the pia mater, CSF communicates freely with interstitial fluid.

Rupture Risk Factors

The decision to treat unruptured aneurysms requires accurate assessment of rupture risk. The ISUIA investigators [47, 148] identified aneurysm size, location, and previous SAH history as major predictors of rupture. Subsequent prospective studies have refined these risk estimates. The PHASES score, developed by Greving et al. [37], incorporates population, hypertension, age, aneurysm size, earlier SAH from another aneurysm, and site to provide individualized rupture risk estimates. Long-term follow-up studies from Finland by Juvela and colleagues [62, 63, 64] have provided valuable data on the natural history of unruptured aneurysms, demonstrating that rupture risk continues over decades and is influenced by smoking and aneurysm size. The UCAS Japan study [94] confirmed size-dependent rupture risk and identified location-specific differences, with anterior communicating artery and posterior communicating artery aneurysms showing higher rupture rates. Sonobe et al. [132] conducted the Small Unruptured Aneurysm Verification (SUAVe) study in Japan, focusing on small aneurysms (<5 mm) and finding that even these lesions have non-negligible rupture risk, particularly in young patients and those with multiple aneurysms.

Clinical Presentation and Outcomes

Ruptured aneurysms typically present with sudden severe headache, often described as “thunderclap” headache, and may be associated with focal neurological deficits, loss of consciousness, or seizures [67, 154]. The International Cooperative Study on the Timing of Aneurysm Surgery [67] provided comprehensive data on management outcomes following SAH. Al-Khindi et al. [1] reviewed cognitive and functional outcomes after aneurysmal SAH, highlighting that even patients with good neurological recovery often experience cognitive deficits affecting quality of life. The management of ruptured aneurysms involves either surgical clipping or endovascular coiling, with the choice influenced by aneurysm morphology, location, and patient factors [32, 106]. The long-term outcomes of patients with SAH remain suboptimal, with many survivors experiencing persistent cognitive and functional impairments [1, 113].

Computational Fluid Dynamics Methodology

Image Acquisition and Segmentation

Patient-specific CFD modeling begins with medical imaging to obtain vascular geometry. Various imaging modalities have been employed, each with advantages and limitations [39, 116]. Three-dimensional rotational angiography (3DRA) offers the highest spatial resolution for cerebrovascular imaging and is considered the gold standard for aneurysm morphology assessment [34, 104, 112]. Computed tomography angiography (CTA) provides rapid acquisition and is widely available, though with lower contrast resolution than 3DRA [34, 112]. Magnetic resonance angiography (MRA), including time-of-flight (TOF) and contrast-enhanced techniques, offers non-invasive imaging without ionizing radiation [44, 48, 50, 56]. Geers et al. [34] compared the reproducibility of CFD hemodynamics derived from CTA and 3DRA, finding generally good agreement but noting that imaging modality influences quantitative WSS values. Similarly, Ren et al. [112] compared 3DRA and CTA for CFD modeling and reported that while geometric differences exist, hemodynamic parameters show reasonable correlation between modalities. The segmentation process converts imaging data into three-dimensional surface models suitable for mesh generation. Cebral and Lohner [12] described early approaches to image-based mesh generation for CFD. Sazonov and Nithiarasu [117] developed semi-automatic surface and volume mesh generation techniques specifically for subject-specific biomedical geometries. The Multiple Aneurysms Anatomy Challenge 2018 (MATCH) organized by Berg et al. [5] evaluated segmentation approaches across multiple centers, revealing significant variability in segmentation outcomes and highlighting the need for standardized protocols. Patient-specific CFD modeling begins with medical imaging to obtain vascular geometry. Various imaging modalities have been employed, each with distinct advantages and limitations for hemodynamic analysis.

Table 1: Comparison of Imaging Modalities for Patient-Specific CFD Modeling.

Modality	Spatial Resolution	Hemodynamic Detail	Key Limitations	Primary Use
3D Rotational Angiography (3DRA)	< 0.3 mm	Very High	Invasive, radiation	Gold standard for morphology
CT Angiography (CTA)	0.5 mm	High	Radiation, less contrast	Widely available, fast acquisition
MR Angiography (MRA-TOF)	0.5–1 mm	Moderate	Long scan time, flow artifacts	No radiation, soft-tissue contrast
Contrast-Enhanced MRA	0.5 mm	High	Gadolinium injection	Better coverage than TOF-MRA
4D Flow MRI (3T)	1.5–2 mm	Low–Moderate	Velocity aliasing, long scan	In vivo hemodynamics, validation tool
4D Flow MRI (7T)	0.7–1 mm	Moderate	Limited availability, cost	Highest in vivo resolution for flow

Mesh Generation and Quality

The accuracy of CFD simulations depends critically on mesh quality. Steinman et al. [133] organized the ASME 2012 Summer Bioengineering Conference CFD Challenge, which compared solutions for pressure and flow in a giant aneurysm across multiple research groups using different solvers and mesh strategies. This landmark study revealed that despite variations in numerical approaches, consistent results could be achieved with adequate mesh resolution. Khan et al. [68] systematically investigated the impact of solver numerics versus mesh and time-step resolution on aneurysm hemodynamics, concluding that mesh and temporal resolution are more critical determinants of accuracy than solver specifics. Valen-Sendstad and Steinman [152] demonstrated that insufficient mesh resolution can lead to erroneous prediction of turbulent flow and inaccurate WSS estimates. The 2015 International Aneurysm CFD Challenge [150] further examined real-world variability in WSS prediction, finding that while qualitative flow patterns were consistent across participants, quantitative WSS values showed considerable variation depending on mesh strategies and numerical schemes. Substantial variability exists across CFD studies, stemming from multiple stages of the modeling pipeline. Table 2 summarizes the major uncertainty sources, their estimated magnitudes, and recommended mitigation strategies.

Table 2: Major Sources of Uncertainty in Patient-Specific CFD Modeling.

Uncertainty Source	Parameter Affected	Magnitude of Error	Mitigation Strategy	Impact Level
Imaging Modality	Geometry reconstruction	Up to 15–20% difference in WSS between CTA vs 3DRA	Use 3DRA as standard; protocol standardization	high
Image Segmentation	Lumen geometry, wall thickness	Significant (MATCH study: inter-operator variability)	Semi-automatic tools; consensus protocols	high
Mesh Resolution	Near-wall WSS accuracy	Factor of 2–5× in WSS depending on mesh density	Mesh independence studies; >3M elements for WSS	High
Inlet Boundary Condition	Velocity/flow rate at inlet	10–30% WSS variation; patient-specific vs. generalized	PC-MRI flow measurement; phase-averaged waveforms	moderate
Outlet Boundary Condition	Pressure distribution	Influences flow splitting; affects WSS in branches	Windkessel/ impedance boundary conditions	moderate
Fluid Viscosity Model	Non-Newtonian vs Newtonian	Most significant in low-shear aneurysm dome regions	Non-Newtonian (Carreau or Walburn-Schneck) for low-flow areas	low– moderate

Boundary Conditions

Boundary conditions represent one of the most important sources of uncertainty in patient-specific CFD modeling [135]. Inlet boundary conditions typically specify velocity or flow rate waveforms at the proximal arteries. Jansen et al. [59] compared generalized versus patient-specific inflow boundary conditions and found that while generalized conditions may suffice for some applications, patient-specific flow rates improve accuracy for quantitative hemodynamic parameters. Outflow boundary conditions are equally important and more challenging due to the distributed nature of cerebral circulation. Chnafa et al. [19] proposed a rational approach for minimizing the impact of outflow strategy on cerebrovascular simulations, demonstrating that impedance-based boundary conditions provide more physiologic flow distributions than simple pressure outlets. Vignon-Clementel et al. [160] developed coupled multidomain methods for outflow boundary conditions in cardio-

vascular simulations, including Wind Kessel models that account for distal vascular resistance and compliance. The Wind Kessel model has been widely applied in cardiovascular hemodynamics [40] and adapted for cerebral circulation. Bit et al. [8] investigated realistic outlet boundary conditions for stenosed arteries, demonstrating their importance for accurate hemodynamic assessment. Figure 4 reiterates the concept of the outer brain barrier (OBB) formed by the arachnoid mater. The image emphasizes the structural distinction between the fenestrated capillaries of the dura mater and the tight junctions of the arachnoid barrier cells. It serves as a visual reminder of the multiple protective layers that encapsulate the central nervous system, with the final layer allowing for free communication between CSF and interstitial fluid beneath the pia mater.

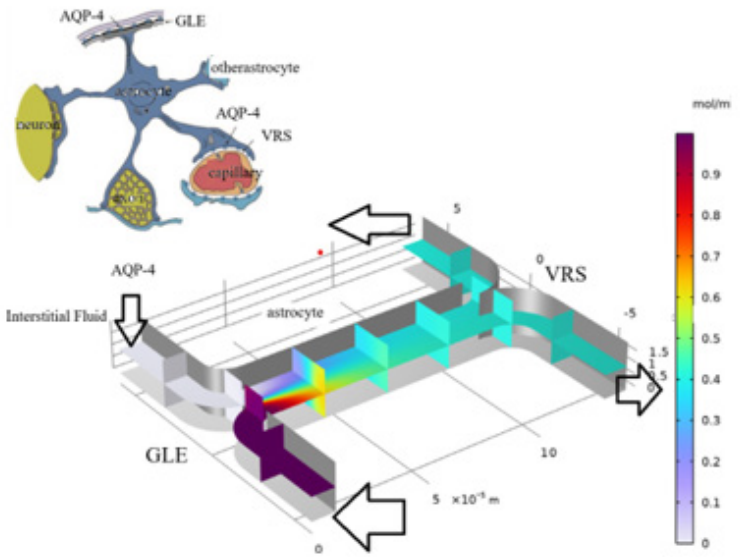

Figure 4: The arachnoid mater establishes the outer brain barrier. While capillaries in the dura mater are fenestrated, tight junctions between arachnoid barrier cells form the outer brain barrier (OBB). Vessels in the subarachnoid space are sealed by their tunica, and capillaries within the barrier have tight endothelium. Below the pia mater, CSF communicates freely with interstitial fluid.

Fluid Properties: Newtonian Vs. Non-Newtonian Models

Blood exhibits non-Newtonian behavior due to its cellular components and plasma proteins, with viscosity dependent on shear rate [95]. The choice between Newtonian and non-Newtonian fluid models has been extensively investigated in cardiovascular CFD. Cho and Kensey [20] examined non-Newtonian effects in diseased arterial vessels, demonstrating significant differences in velocity profiles and wall shear stress compared to Newtonian assumptions. Walburn and Schneck [162] developed constitutive equations for whole human blood that have been widely adopted in CFD studies. Jahangiri et al. [57] compared multiple non-Newtonian models in stenosed arteries, finding that model choice influences hemodynamic factors. Liu et al. [84] specifically compared Newtonian and non-Newtonian models in patients with intracranial arterial stenosis, concluding that non-Newtonian effects are most pronounced in low-shear regions. Kumar et al. [75] performed transient analysis comparing Newtonian and non-Newtonian blood flow in the human aorta. Wei et al. [165] investigated non-Newtonian effects in Fontan hemodynamics, while Mahalingam et al. [86] examined turbulence transition effects in coronary arteries.

Numerical Methods and Solvers

Various numerical methods have been applied to cerebral aneurysm hemodynamics. The finite volume method, implemented in commercial solvers such as ANSYS Fluent and CFX, remains widely used [58, 105, 111]. The finite element method offers advantages for complex geometries and fluid-structure interaction [144, 160]. The lattice Boltzmann method has gained attention for its computational efficiency and ability to handle complex boundaries [58]. Girfoglio et al. [35] developed non-intrusive reduced-order models for patient-specific aortic blood flow. Philip et al. [105] compared idealized and patient-specific geometries for bifurcation aneurysms using finite volume methods. Jain et al. [58] compared lattice Boltzmann simulations with ANSYS solutions and MR imaging for transitional hemodynamics in aneurysms. Figure 5 illustrates the complete patient-specific CFD modeling workflow, from medical image acquisition through to clinical translation, with key uncertainty sources highlighted at each stage.

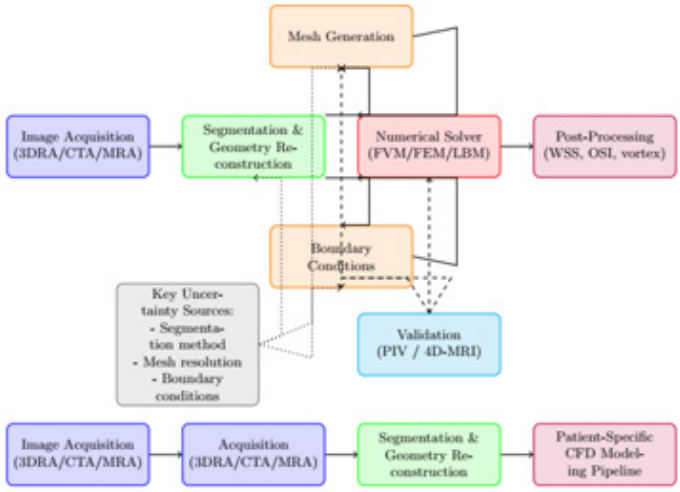

Figure 5: Patient-specific CFD modeling pipeline and major uncertainty sources at each stage.

Hemodynamic Parameters in Aneurysm Assessment

Wall shear stress (WSS) and its spatiotemporal derivatives have emerged as the most extensively studied hemodynamic parameters in relation to aneurysm pathobiology. Table 3 provides a comparative summary of the key hemodynamic parameters, their units, rupture-associated thresholds, pathobiological mechanisms, and evidence strength.

Table 3: Key Hemodynamic Parameters: Clinical and Pathobiological Summary.

Parameter	Unit	Rupture- Associated Threshold	Pathobiological Mechanism	Clinical Relevance	Evidence Strength
Wall Shear Stress (WSS)	Pa	Low (<1.5) or High (>10)	Endothelial dysfunction, remodeling	Most studied; bidirectional rupture role	high
Oscillatory Shear Index (OSI)	— (0 to 0.5)	High (>0.2)	Disturbed flow, atherosclerosis, wall degeneration	Complements WSS; identifies flow reversal	high
Relative Residence Time (RRT)	s/Pa	High (combined Low WSS + high OSI)	Thrombus formation, prolonged exposure	Integrated risk metric; growing use	moderate
Pressure Loss Coefficient (PLc)	—	Elevated	Wall stress, aneurysm expansion	Rupture risk proxy; less validated	moderate
Inflow Jet Velocity	m/s	Concentrated high-speed jet	Impingement, localized wall stress	Feature of ruptured aneurysms	moderate
Flow Complexity Index	—	High complexity	Vortex instability, wall fatigue	Qualitative; often correlated with rupture	moderate

Wall Shear Stress

Wall shear stress, the tangential force exerted by flowing blood on the endothelial surface, is the most extensively studied hemodynamic parameter in cerebral aneurysms [87, 122, 126]. Shojima et al. [126] performed CFD analysis of 20 middle cerebral artery aneurysms and found that WSS was significantly lower in aneurysms compared to parent arteries, with ruptured aneurysms exhibiting lower WSS than unruptured lesions. The relationship between WSS and aneurysm rupture has been debated, with some studies supporting low WSS as a rupture risk factor [10, 61, 93, 126] and others implicating high WSS [71, 91]. Meng et al. [91] proposed a unifying hypothesis suggesting that both low and high WSS can contribute to aneurysm pathobiology through different mechanisms: low WSS promotes inflammatory remodeling and degeneration, while high WSS triggers endothelial-mediated mural weakening. Boussel et al. [10] performed longitudinal imaging of growing aneurysms and found that regions of aneurysm growth corresponded to areas of low WSS at baseline. Jou et al. [61] compared WSS in ruptured and unruptured internal carotid artery aneurysms, finding lower WSS in ruptured lesions. Miura et al. [93] confirmed that low WSS is in-

dependently associated with rupture status in middle cerebral artery aneurysms. Conversely, Cebral et al. [14] found that ruptured aneurysms were characterized by complex flow patterns and concentrated inflow jets, often associated with high WSS regions.

Kono et al. [71] examined hemodynamics at rupture sites and identified high WSS as a feature of the rupture location. Figure 6 showcases the power of computational fluid dynamics (CFD) in assessing hemodynamic parameters across various aneurysm types and locations. It presents simulated data for velocity, wall shear stress (WSS), oscillatory shear index (OSI), and relative residence time in aneurysms of the intracranial arteries (e.g., ICA, MCA), the thoracic aorta, the abdominal aorta (AAA), and coronary arteries (CAA). The figure visually demonstrates how flow patterns and biomechanical forces can be quantified and compared in patient-specific geometries, highlighting the versatility of CFD as a diagnostic tool.

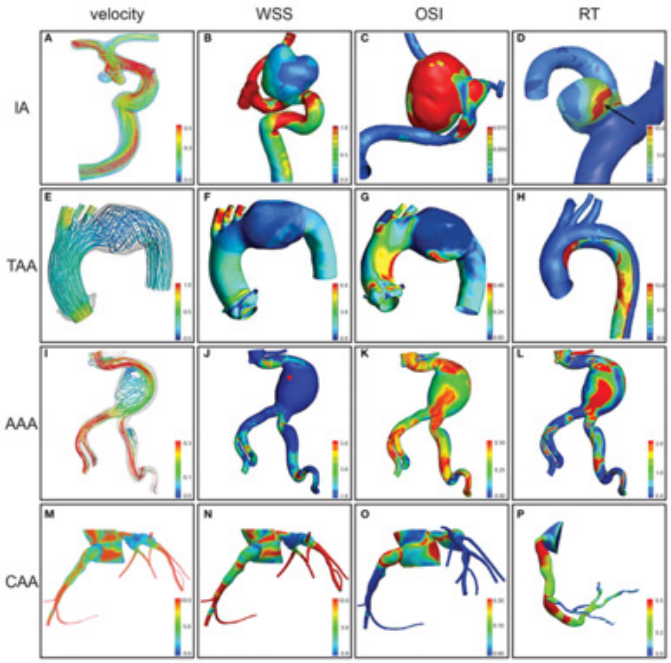

Figure 6: Hemodynamic parameters (velocity, wall shear stress, oscillatory shear index, residence time) assessed by computational modeling for aneurysms at different anatomical locations: intracranial (ICA, paraclinoid, MCA), thoracic (distal arch, dissecting), abdominal (AAA), and coronary (CAA).

Oscillatory Shear Index and Other WSS Derivatives

The oscillatory shear index (OSI) quantifies the directional changes in WSS during the cardiac cycle and has been associated with atherosclerotic plaque development [74]. Ku et al. [74] originally described the relationship between low and oscillating shear stress and atherosclerosis in the carotid bifurcation. In cerebral aneurysms, high OSI has been proposed as a marker of disturbed flow that may promote wall degeneration [139, 140]. Sugiyama et al. [139] investigated relative residence time, a parameter combining low WSS and high OSI, in intracranial aneurysms and found associations with atherosclerotic changes. The same group [140] examined relative residence time as a risk factor for thrombus formation during aneurysm embolization. The gradient oscillatory number and other WSS derivatives have been explored as potential rupture discriminants [41, 137]. Himburg et al. [41] performed spatial comparisons between WSS measures and endothelial permeability, providing mechanistic insights into how WSS patterns influence vascular biology. The relationship between WSS and aneurysm rupture is paradoxically bidirectional. Meng et al. proposed a unifying hypothesis suggesting that both low and high WSS can contribute to aneurysm pathobiology through distinct mechanisms. Low WSS (below ~1.5 Pa) promotes inflammatory remodeling and macrophage-mediated wall degeneration, while high WSS (above ~10 Pa) triggers endothelial mechanosensing pathways leading to mural weakening. Figure 7 illustrates this dual-pathway framework.

Pressure and Pressure Gradients

While less frequently studied than WSS, intra-aneurysmal pressure and pressure gradients may contribute to wall stress and rupture risk [124, 153]. Shimogonya et al. [124] proposed the pressure loss coefficient as a potential indicator of rupture risk. Valencia et al. [153] analyzed blood flow dynamics in basilar artery aneurysm models, examining both WSS and pressure distributions. Chen et al. [16] characterized WSS and pressure in intracranial atheroscle-

rosis using CFD, demonstrating that both parameters vary with plaque characteristics. Raghavan et al. [109] quantified aneurysm shape and its relationship to rupture risk, indirectly addressing wall stress distributions. Longitudinal studies have demonstrated that aneurysm growth preferentially occurs at regions of low WSS. Figure 8 illustrates the conceptual distribution of growth rate versus WSS across stable, growing, and ruptured aneurysm populations, synthesized from the published literature.

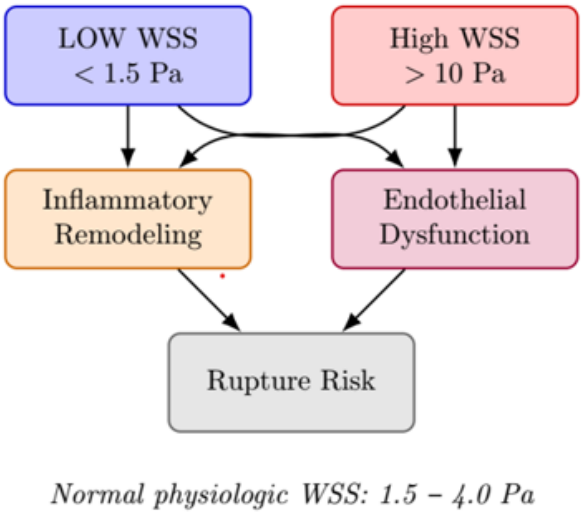

Figure 7: Bidirectional WSS hypothesis: low WSS promotes inflammatory degeneration; high WSS triggers endothelial-mediated mural weakening. Both pathways converge on aneurysm rupture.

Figure 8: Conceptual distribution of aneurysm growth rate versus wall shear stress (Pa). Ruptured aneurysms cluster at both low-WSS and high-WSS extremes, consistent with the bidirectional hypothesis.

Flow Patterns and Complexity

Qualitative flow characteristics, including flow stability, impingement regions, and intra-aneurysmal vortex structures, provide complementary information to quantitative parameters [11, 122]. Cebral et al. [11] characterized cerebral aneurysms for rupture risk assessment using patient-specific hemodynamics, identifying complex flow patterns as features of ruptured aneurysms. Sforza et al. [122, 123] reviewed hemodynamics of cerebral aneurysms and investigated the effects of perianeurysmal environment on flow patterns during growth. Gopalakrishnan et al. [36] analyzed dynamics of pulsatile flow through model abdominal aortic aneurysms, providing insights applicable to cerebral aneurysms. Fukazawa et al. [33] used CFD to characterize local hemodynamic features at middle cerebral artery aneurysm rupture points, finding that rupture sites were associated with specific flow characteristics. Omodaka et al. [102] similarly examined local hemodynamics at rupture points.

Kinetic Energy and Momentum

The kinetic energy and momentum of blood flow entering aneurysms influence intra-aneurysmal hemodynamics and wall loading. Isoda and colleagues have extensively investigated inflow hemodynamics using both CFD and MR-based techniques [51-55]. Their work has characterized the relationship between inflow jet characteristics and aneurysm geometry. Chnafa et al. [18] examined vessel caliber and flow splitting relationships at the internal carotid artery terminal bifurcation, providing reference data for inflow boundary conditions. Seymour et al. [121] measured blood flow rate and WSS in seven major cephalic arteries, establishing normative values for CFD validation.

Morphological Factors and Hemodynamic Interactions

Aneurysm morphology and hemodynamics are tightly coupled: geometric characteristics directly influence intra-aneurysmal flow patterns, while hemodynamic forces drive wall remodeling and shape change over time. Table 4 provides a comprehensive comparison of established morphological risk factors, their thresholds, evidence strength, and clinical significance.

Table 4: Morphological Risk Factors for Aneurysm Rupture: Comparative Summary.

Morphological Factor	Risk Threshold	Evidence Strength	Key References	Clinical Notes
Aneurysm Size	>7 mm (moderate) >25 mm (high)	Strong	ISUIA, UCAS Japan, PHASES score	Most established clinical predictor; size alone insufficient
Aspect Ratio (Dome/Neck)	>1.6	Moderate–Strong	Ujiie et al. 1999, 2001; Dhar et al. 2008	High AR = stagnant flow in dome; requires standardized sizing method
Irregular Shape / Blebs	Any bleb presence	Strong	Raghavan et al. 2005; Chien et al. 2009; Zhang et al. 2016	Blebs correlate with focal low WSS; independent predictor
Location: PComA/ AComA	Posterior Communicating or Anterior Communicating Artery	Strong	UCAS Japan 2012; Greving et al. 2014; Lin et al. 2013	Location-specific hemodynamics; higher rupture rate per PHASES score
Bifurcation vs. Sidewall	Bifurcation type	Moderate	Baharoglu et al. 2012; Chung et al. 2014	Distinct pathomechanisms; morphologic predictors differ by type
Parent Vessel Geometry	High curvature, narrow angle	Moderate	Hoi et al. 2004; Chnafa et al. 2017	Influences inflow jet; non-linear interaction with aneurysm morphology

Aneurysm Size and Shape

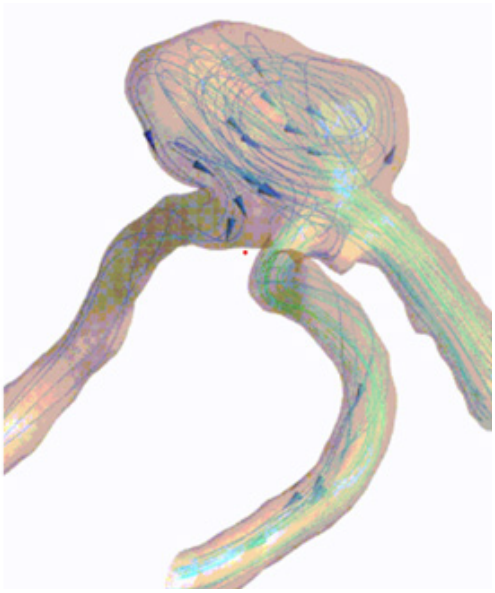

Figure 9: Use of computational fluid dynamics simulations to derive detailed hemodynamic information of high clinical relevance for predicting the risk of cardiovascular and neural diseases, and identifying critical structural and hemodynamic parameters for clinical assessment.

Aneurysm size has long been recognized as a rupture risk factor [27, 47, 62, 148]. Dhar et al. [27] identified morphology parameters for rupture risk assessment, including size, aspect ratio, and bottleneck factor. Ujiie et al. [146, 147] proposed aspect ratio (dome height-to-neck width) as a reliable index for predicting rupture, based on the observation that high aspect ratio aneurysms exhibit more disturbed flow. Raghavan et al. [109] quantified aneurysm shape and demonstrated that irregular shapes are associated with increased rupture risk. Skodvin et al. [129] examined cerebral aneurysm morphology before and after rupture in a nationwide case series, providing unique insights into morphological changes associated with rupture events. Singla et al. [127] developed a CFD-based model for assessing rupture risk in cerebral arteries with varying aneurysm sizes. Lauric et al. [76] demonstrated that rupture status discrimination performance of aspect ratio, height/width, and bottleneck factor is highly dependent on aneurysm sizing methodology. Figure 9 illustrates the clinical translational pathway for computational fluid dynamics (CFD) simulations in neurovascular and cardiovascular medicine. It depicts the process of converting medical images into detailed 3D models to derive clinically relevant hemodynamic information. The ultimate goal, as shown, is to predict disease risk, such as aneurysm rupture, by identifying critical structural and hemodynamic parameters. This workflow underscores the potential of CFD to move beyond research and provide actionable insights for patient-specific clinical assessment and treatment planning.

Aneurysm Location and Type

Aneurysm location influences both natural history and hemodynamic characteristics [26, 37, 94]. Baharoglu et al. [2] identified a dichotomy in morphological predictors of rupture status between sidewall and bifurcation-type intracranial aneurysms, suggesting that different hemodynamic mechanisms may operate in these aneurysm types. Chung et al. [23] compared hemodynamics of saccular and fusiform aneurysms of the basilar artery, finding distinct flow patterns between morphological types. Lin et al. [82, 83] analyzed morphological parameters to differentiate rupture status in anterior communicating artery and middle cerebral artery aneurysms, respectively. Jing et al. [60] examined hemodynamic and morphological characteristics of posterior communicating artery aneurysms. Kono and Terada [72] specifically studied hemodynamics of the anterior communicating artery using CFD. Figure 10 presents a radar-chart visualization of the relative hemodynamic and morphologic risk signatures for ruptured versus unruptured aneurysms, aggregated from the systematic literature reviewed. Ruptured lesions consistently show elevated risk across all dimensions, with the most pronounced differentiation in flow complexity, aspect ratio, and low WSS.

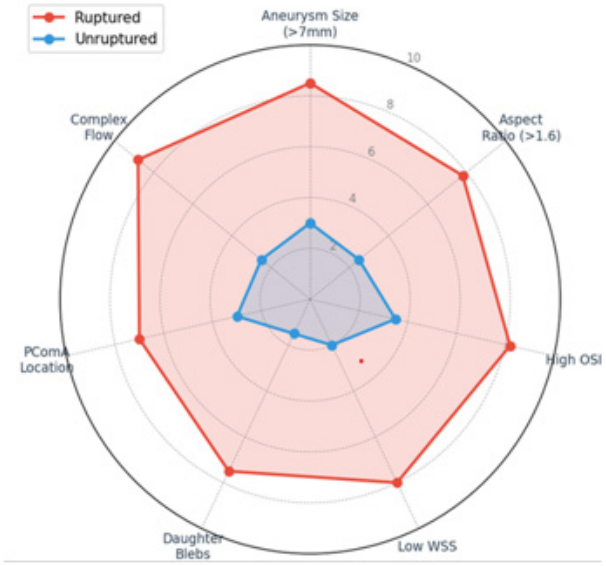

Figure 10: Radar chart comparing the hemodynamic and morphologic risk profiles of ruptured vs. unruptured intracranial aneurysms across seven validated dimensions. Scale: 0–10 (literature-derived evidence scores).

Daughter Blebs and Irregularities

The presence of daughter blebs or irregular protrusions on aneurysm domes has been associated with increased rupture risk [17, 172]. Chien et al. [17] performed patient-specific hemodynamic analysis of small internal carotid artery-ophthalmic artery aneurysms with and without blebs, finding that bleb formation is associated with specific hemodynamic environments. Zhang et al. [172] analyzed hemodynamics of intracranial aneurysms with daughter blebs, demonstrating that blebs are typically located in regions of low WSS and complex flow. Varble et al. [158] examined shared and

distinct rupture discriminants of small and large intracranial aneurysms, including the role of surface irregularities.

Parent Vessel Geometry

The geometry of the parent vessel and its relationship to the aneurysm significantly influences intra-aneurysmal hemodynamics [18, 43, 96, 97]. Hoi et al. [43] studied effects of arterial geometry on aneurysm growth using three-dimensional CFD. Chnafa et al. [18] provided detailed measurements of vessel caliber and flow splitting at the internal carotid artery terminal bifurcation. Nagargoje and colleagues [96, 97] investigated the effects of sinus size and position on hemodynamics in carotid artery bifurcations and analyzed pulsatile flow dynamics in symmetric and asymmetric bifurcating vessels. Usmani and Muralidhar [149] examined unsteady hemodynamics in intracranial aneurysms with varying dome orientations.

Validation of Computational Fluid Dynamics

CFD predictions must be validated against experimental and in vivo measurements to establish their reliability. Two primary validation approaches exist: in vitro validation with particle image velocimetry (PIV) and in vivo validation with phase-contrast MRI techniques. Table 5 provides a detailed comparison of available validation methods.

Table 5: Comparison of CFD Validation Methods: Capabilities, Accuracy, and Use Cases.

Method	Spatial Resolution	Parameter Accuracy	WSS Accuracy	Limitations	Best Use Case
PIV (In Vitro)	0.1–0.3 mm	High velocity accuracy	~2% error for velocity	Cannot reproduce in vivo conditions	Benchmark for new CFD methods
2D Phase-Contrast MRI (PC-MRI)	1–2 mm	Moderate (flow rate)	10–20% WSS error	Limited to 2D planes; no WSS	Flow rate validation; widely used
4D Flow MRI (3T)	1.5–2 mm	Moderate velocity, low WSS	30–50% WSS underestimate	Velocity aliasing; long scan	Clinical validation; routine use
4D Flow MRI (7T)	0.7–1 mm	Best in vivo resolution	~20% WSS error	Limited availability, high cost	Research standard; narrows gap to CFD
Computational (CFD only)	0.01–0.1 mm	Unlimited parameters	Varies 30–80% between centers (WSS)	Assumptions re: geometry, boundary conditions	No gold standard for WSS

In Vitro Validation with Particle Image Velocimetry

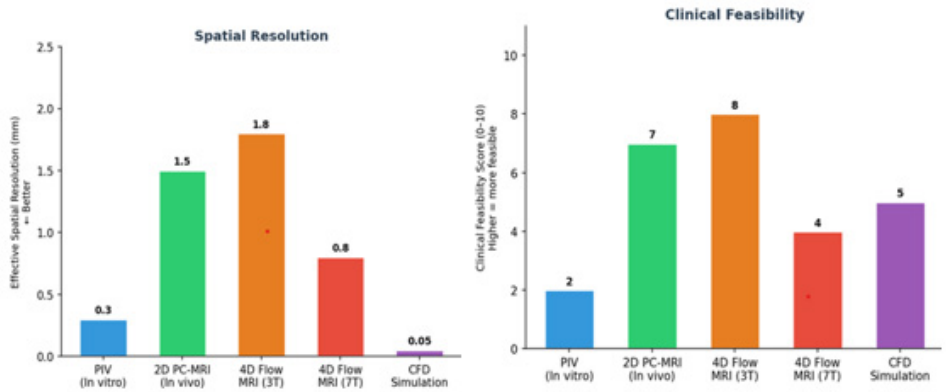

Figure 11: Comparison of CFD validation modalities: spatial resolution (mm, lower is better) and clinical feasibility score (higher is more practical). PIV offers best resolution but lowest clinical feasibility; 4D Flow MRI at 3T provides the optimal balance for routine validation.

Particle image velocimetry (PIV) has been extensively used to validate CFD predictions in idealized and patient-specific aneurysm models [31, 110]. Ford et al. [31] compared PIV-measured and CFD-predicted flow dynamics in anatomically realistic cerebral aneurysm models, finding good qualitative agreement but quantitative differences that highlighted the importance of accurate geome-

try reproduction. Raschi et al. [110] performed combined CFD and PIV analysis of hemodynamics in a growing intracranial aneurysm, using serial imaging to track morphological changes and validate flow predictions. Bhardwaj et al. [7] modeled flow in an in vitro anatomical cerebrovascular model with experimental validation, demonstrating the feasibility of physical modeling for CFD validation. Figure 11 presents a comparison of CFD validation modalities.

In Vivo Validation with Phase-Contrast MRI

Phase-contrast MRI (PC-MRI) and time-resolved 3D phase-contrast MRI (4D Flow MRI) provide the primary means for in vivo validation of CFD predictions [3, 9, 48, 49, 56, 90, 98, 111]. Bammer et al. [3] performed time-resolved 3D quantitative flow MRI of major intracranial vessels, establishing techniques for acquiring velocity fields in vivo. Boussel et al. [9] directly compared PC-MRI measurements and CFD predictions in intracranial aneurysms, demonstrating reasonable agreement for flow patterns and velocity fields while noting discrepancies in WSS quantification. Rayz et al. [111] similarly compared CFD results with in vivo MRI measurements, validating simulation approaches for clinical applications. Isoda and colleagues have made substantial contributions to MR-based hemodynamic assessment [48-56] [70, 171]. Their work has developed magnetic resonance fluid dynamics (MRFD) based on time-resolved 3D phase-contrast MRI and compared these measurements with CFD predictions. Isoda et al. [53] performed in vivo hemodynamic analysis of intracranial aneurysms using MRFD, while subsequent studies compared inflow hemodynamics between CFD and MRFD [51, 52]. Naito et al. [98] compared magnetic resonance fluid dynamics with computed fluid dynamics for intracranial aneurysms. van Ooij et al. [156, 157] estimated WSS with phase-contrast MRI in both in vitro and in vivo settings and developed methodology to detect abnormal relative WSS using 4D Flow MRI.

High-Field MRI and 4D Flow

Higher magnetic field strengths offer improved signal-to-noise ratio and spatial resolution for flow imaging. Berg et al. [6] compared cerebral blood flow CFD with time-resolved 3D phase-contrast MRI at 7T, demonstrating the potential of ultra-high-field MRI for hemodynamic validation. Meckel et al. [90] performed in vivo visualization and analysis of 3D hemodynamics in cerebral aneurysms with flow-sensitized 4D MR imaging at 3T. Markl et al. [89] provided a comprehensive review of 4D Flow MRI techniques and applications. Schnell et al. [120] examined three-dimensional hemodynamics in intracranial aneurysms, investigating the influence of size and morphology on flow patterns. Nett et al. [99] developed accelerated dual velocity encoding techniques for 4D phase-contrast MRI. Takehara et al. [143] assessed the accuracy and reproducibility of 4D Flow MRI for WSS measurements in cerebral aneurysms. Figure 12 demonstrates the application of 4D Flow MRI for visualizing complex hemodynamics, specifically in a case of chronic aortic dissection. The end-systolic streamlines vividly show blood entering the false lumen through a primary entry tear. Correspondingly, the color-coded wall shear stress (WSS) map on the aortic wall reveals elevated hemodynamic forces along the superior wall of the proximal descending aorta, where the flow jet impinges. This image highlights the capability of advanced imaging to provide in vivo validation for CFD models and to identify regions exposed to pathological mechanical stress.

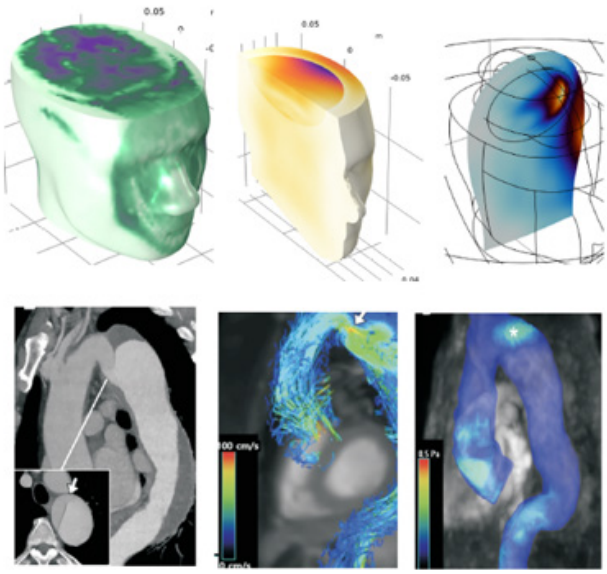

Figure 12: The application of 4D-flow imaging provides valuable insight into hemodynamics in chronic aortic dissection. As shown end-systolic streamlines visualize flow entering the false lumen through the primary entry tear (arrow). Correspondingly, the wall shear stress map demonstrates increased hemodynamic forces along the superior wall of the proximal descending aorta.

Multi-Modality Validation Approaches

Recent studies have employed multi-modality approaches combining CFD, MRI, and other techniques for comprehensive validation. Rutkowski et al. [115] used machine learning to enhance cerebrovascular 4D Flow MRI velocity fields using CFD simulation data. Thomas et al. [145] assessed cerebrovascular responses to physiological stimuli in identical twins using multimodal imaging and CFD. Suh et al. [141] quantified hemodynamic changes in abdominal aortic aneurysms with exercise using MR exercise imaging and CFD, demonstrating the potential for functional hemodynamic assessment.

Clinical Applications and Translational Challenges

Rupture Risk Prediction

The ultimate goal of hemodynamic analysis is to improve rupture risk prediction beyond what is possible with clinical and morphological factors alone [26, 107, 119, 142, 169]. Cebral et al. [14] quantitatively characterized hemodynamic environments in ruptured and unruptured brain aneurysms, identifying flow complexity and concentrated inflow jets as features of ruptured lesions. Xiang et al. [169] developed hemodynamic-morphologic discriminants for intracranial aneurysm rupture, finding that low WSS and high oscillatory shear index were associated with ruptured aneurysms. Takao et al. [142] examined hemodynamic differences between unruptured and ruptured aneurysms during observation. Schneiders et al. [119] evaluated the additional value of intra-aneurysmal hemodynamics in discriminating ruptured versus unruptured aneurysms, finding that hemodynamic parameters improved classification beyond morphological factors alone. Detmer et al. [26] analyzed associations of hemodynamics, morphology, and patient characteristics with aneurysm rupture stratified by location.

Treatment Planning and Device Design

CFD has been applied to simulate the hemodynamic effects of endovascular treatments, including coiling and flow diversion [25, 42, 73]. Hodis et al. [42] studied the relationship between aneurysm occlusion and flow diverters using CFD. De Santis et al. [25] investigated the hemodynamic impact of stent-vessel malapposition following carotid artery stenting. Krings et al. [73] examined partial targeted embolization of brain arteriovenous malformations. Gundert et al. [38] used CFD to identify optimal stent design parameters for reducing WSS gradients in coronary arteries, an approach applicable to cerebrovascular stents.

Growth and Remodeling Prediction

Longitudinal studies have begun to elucidate the relationship between hemodynamics and aneurysm growth [10, 101, 110, 138]. Boussel et al. [10] demonstrated that aneurysm growth occurs at regions of low WSS in a patient-specific longitudinal study. Raschi et al. [110] analyzed hemodynamics in a growing intracranial aneurysm using serial imaging and CFD. Sugiyama et al. [138] performed hemodynamic analysis of growing intracranial aneurysms arising from the posterior inferior cerebellar artery. Nordahl et al. [101] examined morphological and hemodynamic changes during cerebral aneurysm growth. Cebral and Raschi [15] reviewed suggested connections between risk factors of intracranial aneurysms, integrating hemodynamic, morphological, and clinical factors.

Machine Learning and Big Data Approaches

The increasing availability of hemodynamic data has stimulated interest in machine learning approaches for rupture risk prediction [115, 128]. Sinnaswamy et al. [128] provided an extensive review of deep learning and machine learning interventions in prediction and classification of aneurysm types. Rutkowski et al. [115] demonstrated the use of machine learning to enhance 4D Flow MRI velocity fields using CFD simulation data, suggesting potential for hybrid approaches combining imaging and computation. Table 6 presents a structured roadmap for clinical translation, mapping current barriers to proposed solutions with realistic timelines and current development status. Machine learning approaches are increasingly being applied to integrate large-scale hemodynamic data with clinical outcomes [115, 128]. These methods offer the potential to identify complex, non-linear relationships between hemodynamic parameters and rupture risk that may not be apparent through traditional statistical approaches.

Table 6: Clinical Translation Roadmap: Challenges, Solutions, and Timelines.

Challenge	Current Barrier	Proposed Solution	Timeline	Status
Imaging Protocol Standardization	Multi-center segmentation variability	Consensus imaging protocols; MATCH inititative model	NEAR-TERM (1–3 years)	Ongoing
CFD Parameter Standardization	Inter-center WSS variability 30–80%	Reporting guidelines; reference benchmarks	NEAR-TERM (1–3 years)	In Progress
Prospective Multicenter Validation	Lack of prospective rupture outcome data	Large-scale cohort with hemodynamic baseline and follow-up	MID-TERM (3–7 years)	Planned/ Ongoing
Machine Learning Integration	Time-consuming simulations (hours per case)	ML surrogate models; accelerated CFD; hybrid pipelines	MID-TERM (3–7 years)	Research Phase
Clinical Decision Support Tool	Clinician accessibility; complex metrics	Simplified scores (PHASES+ hemodynamics); AI-assisted reports	LONG-TERM (5–10 years)	Conceptual
FSI / Multiscale Modeling	Rigid wall assumption; molecular processes omitted	Fluid-structure interaction + wall biology models	LONG-TERM (5–10 years)	Research Phase

Challenges in Clinical Translation

Despite decades of research, hemodynamic analysis has not yet become standard clinical practice for aneurysm management. Berg et al. [4] reviewed the reliability of hemodynamic modeling in intracranial aneurysms, concluding that CFD alone cannot solve the clinical equation. Chung and Cebral [22] reviewed proposed clinical uses of CFD and their challenges, identifying issues related to standardization, validation, and interpretability. Steinman and Pereira [135] provided an overview of sources of error and variability in patient-specific computational models of cerebral aneurysms. Valen-Sendstad et al. [150] documented real-world variability in aneurysm WSS prediction through the 2015 International Aneurysm CFD Challenge. Maramkandam et al. [88] proposed a novel parameter for rupture risk prediction based on morphology, potentially simplifying the translation of hemodynamic insights to clinical practice.

Emerging Technologies and Future Directions

Fluid-Structure Interaction

Fluid-structure interaction (FSI) models incorporate vessel wall compliance and deformation, potentially providing more realistic assessments of wall stress [105, 123, 144]. Philip et al. [105] examined hemodynamics and biomechanics of morphologically distinct saccular intracranial aneurysms, comparing idealized and patient-specific geometries. Sforza et al. [123] investigated effects of perianeurysmal environment during aneurysm growth, indirectly addressing the role of surrounding structures in constraining deformation. Taylor and Figueroa [144] reviewed patient-specific modeling of cardiovascular mechanics, including FSI approaches.

Multiscale Modeling

The integration of cellular and molecular processes with continuum hemodynamics represents a frontier in aneurysm research [21, 45, 46, 78, 79]. Choudhury et al. [21] studied transport and interaction between blood flow and low-density lipoprotein in near-wall regions. Hoque et al. [45, 46] used dissipative particle dynamics to simulate red blood cells in flow through constricted channels and bifurcations. Lei et al. [78] developed methods for direct construction of mesoscopic models from microscopic simulations. Leng et al. [79] used CFD modeling of symptomatic intracranial atherosclerosis to predict stroke recurrence risk.

Porous Media Modeling

Some investigators have applied porous media modeling to simulate blood flow in regions with complex geometry, such as partially thrombosed aneurysms or tissue-engineered constructs [28, 29, 163, 166]. Ergun [28] and Ergun and Orning [29] developed fundamental equations for fluid flow through packed columns that have been adapted for biological applications. Whitaker [166] provided theoretical derivations of Darcy's law for flow in porous media, while Wang et al. [163] developed volume-averaged macroscopic equations for fluid flow in moving porous media.

Multicenter Initiatives and Standardization

The recognition of variability in CFD methods has led to multicenter initiatives aimed at standardization and reproducibility [5, 133, 150]. The ASME 2012 CFD Challenge [133] demonstrated that with careful attention to numerical parameters, consistent results could be achieved across different solvers and research groups. The 2015 International Aneurysm CFD Challenge [150] revealed persistent variability in WSS prediction and identified sources of discrepancy. The Multiple Aneurysms Anatomy Challenge 2018 (MATCH) [5] focused specifically on segmentation variability, demonstrating that geometric reconstruction remains a major source of uncertainty in patient-specific modeling. These initiatives have informed recommendations for best practices and reporting standards.

Discussion

Summary of Key Findings

This comprehensive review synthesizes the extensive literature on cerebral aneurysm hemodynamics, encompassing over 170 studies spanning from epidemiological observations to advanced computational modeling. Several key themes emerge from this body of work. First, the hemodynamic environment within intracranial aneurysms is complex and patient-specific, influenced by aneurysm morphology, parent vessel geometry, and physiologic flow conditions [11, 12, 13, 122]. Computational fluid dynamics has matured into a powerful tool for quantifying this environment, providing detailed measurements of velocity fields, wall shear stress, and derived parameters that are not accessible through clinical imaging alone [9, 13, 111, 144].

Second, wall shear stress and its spatiotemporal derivatives have emerged as the most extensively studied hemodynamic parameters in relation to aneurysm pathobiology [10, 61, 87, 91, 93, 126]. However, the relationship between WSS and rupture risk is complex, with both low and high WSS implicated through different mechanistic pathways [91]. This complexity likely reflects the multifactorial nature of aneurysm progression, involving endothelial dysfunction, inflammatory remodeling, and mural weakening [15, 92, 125].

Third, morphological characteristics including aneurysm size, aspect ratio, location, and the presence of daughter blebs interact with hemodynamics to influence rupture risk [2, 23, 26, 27, 60, 76, 82, 83, 146, 147, 158, 172]. These interactions underscore the importance of integrating morphological and hemodynamic assessments for comprehensive risk stratification [26, 119, 169]. Fourth, validation studies comparing CFD with in vitro PIV measurements [7, 31, 110] and in vivo phase-contrast MRI [3, 9, 48, 49, 53, 56, 90, 98, 111, 156] have generally demonstrated good qualitative agreement while revealing quantitative discrepancies that highlight sources of uncertainty. High-field MRI at 7T offers enhanced resolution for validation [6], and 4D Flow MRI techniques continue to advance [89, 99, 115, 143]. Fifth, despite decades of research and thousands of patient-specific simulations, hemodynamic anal-

ysis has not yet achieved widespread clinical adoption [4, 22, 135]. Challenges include methodological variability across centers [5, 68, 133, 150, 152], uncertainty regarding which parameters most strongly predict outcomes, and the need for prospective validation in clinical cohorts.

Sources of Variability and Uncertainty

Understanding the sources of variability in hemodynamic modeling is essential for interpreting study results and advancing toward clinical applications [135]. Image acquisition and segmentation introduce geometric uncertainty that propagates through the modeling pipeline [5, 34, 104, 112]. Mesh resolution and numerical schemes influence quantitative results, particularly for WSS which is sensitive to near-wall grid resolution [68, 133, 150, 152]. Boundary conditions represent another major source of uncertainty [59, 135, 160]. While patient-specific flow rates improve accuracy [59], such data are often unavailable, necessitating generalized or literature-based conditions [121]. Outflow boundary conditions are particularly challenging in the cerebral circulation due to the complexity of distal vascular beds and collateral pathways [19, 160]. Fluid properties, including the choice between Newtonian and non-Newtonian models, affect results in low-shear regions such as aneurysm domes [20, 57, 75, 84, 86, 162, 165]. However, the magnitude of these effects relative to other sources of uncertainty remains debated.

Toward Clinical Translation

The translation of hemodynamic analysis to clinical practice will require addressing several fundamental challenges [4, 22, 135]. Standardization of imaging protocols, segmentation methods, mesh generation, and numerical parameters is essential for ensuring reproducibility across centers and over time. The development of reporting guidelines and quality metrics would facilitate comparison across studies and meta-analysis of accumulated data. Prospective multicenter studies are needed to establish the predictive value of hemodynamic parameters beyond established clinical and morphological risk factors [26, 37, 94, 119, 142, 169]. Such studies should employ standardized methodologies and include sufficiently large patient populations with long-term follow-up to capture rupture events. The integration of hemodynamic analysis with emerging technologies, including machine learning [115, 128], multiscale modeling [21, 45, 46, 78], and fluid-structure interaction [105, 123, 144], may enhance predictive capability. Simplified parameters derived from complex simulations [88, 124] could facilitate clinical implementation by reducing computational requirements and improving interpretability.

Limitations of This Review

This review, while comprehensive, has several limitations. The literature on cerebral aneurysm hemodynamics is extensive, and despite our efforts to include representative studies, some relevant work may have been omitted. The focus on English-language publications may exclude important contributions in other languages. The rapid pace of methodological development means that some emerging techniques may not be fully represented. More aspects of CFD calculation can mentioned in following references: The investigation of blood flow dynamics under various physical conditions represents a significant contribution to cardiovascular research. Early work established fundamental understanding of non-Newtonian blood behavior in magnetohydrodynamic pumps [175], providing foundation for subsequent magnetic field applications in medicine. The analysis of biomagnetic Carreau fluid flow through stenosed arteries with magnetic heat transfer [177] advanced the understanding of magnetic targeting for cardiovascular interventions. Complementary research examined oxygenated and deoxygenated blood flow through tapered stenosed arteries under magnetic field influence [178], revealing important differences in flow characteristics based on blood oxygenation states. Thermal radiation and viscous effects on entropy generation in forced convection blood flow over axisymmetric stretching sheets [179] provided insights into energy dissipation in cardiovascular systems. Numerical investigation of viscous heating effects in renal artery stenosis under peristaltic wall motions [185] addressed kidney-specific hemodynamics, while energy harvesting via micro-turbines in blood arteries [190] explored innovative power generation for implantable bio-devices.

A major research theme involves developing and optimizing drug delivery mechanisms. Microrobots propulsion system design for targeted drug delivery [182] established theoretical frameworks for microscopic medical interventions. Magnetic field effects on silver nanoparticles for drug and gene delivery in biological systems [181] demonstrated the potential of magnetic targeting. Optimal design of magnetic fields for reaction control in drug delivery applications [184] provided optimization methodologies for treatment planning. Fluid-solid interaction modeling of cerebrospinal fluid absorption in arachnoid villi [183] addressed neurological drug delivery pathways. The investigation of magnetohydrodynamic effects on natural silver nanoparticles for pharmaceutical compound transport [189] combined nanotechnology with magnetic guidance. Olfactory drug aerosol delivery with acoustic radiation [176] and numerical modeling of olfactory drug delivery with acoustic streaming [202] pioneered non-invasive brain-targeting approaches through the nasal pathway. Comprehensive toxicity studies established safety profiles for nanoparticle-based medical applications. Research on silver nanoparticles synthesized from seaweed Sargassum angustifolium in common carp (Cyprinus carpio) [180] provided foundational ecotoxicity data. Similar investigations in Barbus sharpeyi [186] expanded the toxicity database across species. Magnetic field effects on silver nanoparticle-induced oxidative stress and apoptosis [188] revealed important interactions between magnetic targeting and cellular responses.

Development and analysis of medical devices represents a significant contribution area. Flow analysis in magnetohydrodynamic pumps for blood circulation [175] supported artificial heart and bypass technologies. Inspiratory leakage flow fraction for surgical masks with varying gaps and filter materials [173] addressed critical public health needs during respiratory disease outbreaks. Use of nanoparticle-enhanced phase change material for cooling surface acoustic wave sensors [187] improved medical sensing device

performance. Energy harvesting from blood flow using micro-turbines [190] explored self-powered implantable devices. Research on surgical mask performance [173] provided quantitative understanding of respiratory protection mechanisms. Bubble growth dynamics in pool boiling [174], while primarily thermal engineering research, has applications in understanding gas exchange in biological fluids and respiratory therapeutics. Three-dimensional lattice Boltzmann modeling of bubble growth [174] established computational methods applicable to microfluidic medical devices. Droplet formation in microfluidic T-junctions [191] provided fundamental understanding for lab-on-chip diagnostic and therapeutic systems. Effect of injection angle, density ratio, and viscosity on droplet formation [191] optimized microfluidic device design for biomedical applications. Advanced computational approaches addressed specific disease mechanisms and therapies. A molecular key to the filter: podocin phosphorylation in early-stage steroid-resistant nephrotic syndrome [192] combined molecular modeling with clinical nephrology. Conservative numerical framework for nonlinear ultrasound propagation in thermo-viscous tissue phantoms [193] advanced therapeutic ultrasound applications. Comprehensive review of computational modeling in tumor and brain disorders with focus on ablation therapies [194] synthesized knowledge for oncology applications.

Numerical investigation of temperature fields in hyperthermia considering diffusion in interstitial tissue [199] optimized cancer thermal therapy protocols. Parameter study of J-integral over craze lines in root-canalled teeth [201] applied fracture mechanics to dental biomechanics. Electrohydrodynamic squeeze-film interaction in synovial joints [200] addressed joint lubrication mechanisms with implications for arthritis treatment. Recent work explores cutting-edge biomedical applications. Cracking the molecular matrix: next-gen AI reshapes biomedicine [195] reviewed artificial intelligence applications in medical research. Smart lubrication for joints using carbon nanomaterials [196] investigated advanced materials for orthopedic applications. Comprehensive review on deep learning for genomics and AI in drug discovery [197] synthesized computational approaches for pharmaceutical development. Superiority of carbon nanocomposites on diarthrosis lubrication [198] extended nanomaterial applications to joint therapy. International dissemination of medical research included presentations on olfactory drug delivery [202] and pool boiling applications in biomedical contexts [203], demonstrating engagement with the global scientific community.

Conclusions

Cerebral aneurysm hemodynamics represents a mature field of investigation with over two decades of active research. Computational fluid dynamics has provided unprecedented insight into the flow environment within intracranial aneurysms and its relationship to aneurysm initiation, growth, and rupture. Wall shear stress and related parameters have emerged as key hemodynamic factors, though their precise role in rupture risk stratification remains incompletely defined. Significant progress has been made in validating CFD predictions against in vitro and in vivo measurements, and multicenter initiatives have begun to address issues of variability and reproducibility. However, translation to routine clinical practice awaits further standardization, prospective validation, and the development of simplified approaches that can be integrated into clinical workflow. The integration of hemodynamic analysis with clinical, morphological, and emerging molecular biomarkers holds promise for improving the management of patients with unruptured intracranial aneurysms, enabling more accurate identification of lesions at highest risk of rupture and appropriate selection for preventive treatment.

Acknowledgment

None.

Funding

None.

Conflict of Interest

No conflict of interest.

References

1. Al-Khindi T, Macdonald RL, Schweizer TA (2010) Cognitive and functional outcome after aneurysmal subarachnoid hemorrhage. Stroke 41(8):e519-e536.
2. Baharoglu MI, Lauric A, Gao B-L, Malek AM (2012) Identification of a dichotomy in morphological predictors of rupture status between sidewall-and bifurcation-type intracranial aneurysms. J Neurosurg 116(4):871-881.
3. Bammer R, Hope TA, Aksoy M, Alley MT (2007) Time-resolved 3D quantitative flow MRI of the major intracranial vessels: initial experience and comparative evaluation at 1.5T and 3T in combination with parallel imaging. Magn Reson Med 57:127-140.
4. Berg P, Saalfeld S, Voß S, Beuing O, Janiga G (2019) A review on the reliability of hemodynamic modeling in intracranial aneurysms: why computational fluid dynamics alone cannot solve the equation. Neurosurg Focus 47(1):15.
5. Berg P, Voß S, Saalfeld S, et al. (2018) Multiple aneurysms anatomy challenge 2018 (match): Phase I: segmentation. Cardiovascular Eng Technol 9: 565-581.
6. Berg P, Stucht D, Janiga G, Beuing O, Speck O, et al. (2014) Cerebral blood flow in a healthy Circle of Willis and two intracranial aneurysms: computational fluid dynamics versus time-resolved 3D phase-contrast MRI at 7T. J Magn Reson Imaging 40:942-950.
7. Bhardwaj S, Craven BA, Sever JE, Costanzo F, Simon SD, et al. (2023) Modeling flow in an in vitro anatomical cerebrovascular model with experimental validation. Front Med Technol 5:1130201.
8. Bit A, Alblawi A, Chattopadhyay H, et al. (2020) Three-dimensional numerical analysis of hemodynamic of stenosed artery considering realistic outlet boundary conditions. Comput Methods Prog Biomed 185:105163.
9. Boussel L, Rayz V, Martin A, et al. (2009) Phase-contrast magnetic resonance imaging measurements in intracranial aneurysms in vivo of flow patterns, velocity fields, and wall shear stress: comparison with computational fluid dynamics. Magn Reson Med 61:409-417.
10. Boussel L, Rayz V, McCulloch C, et al. (2008) Aneurysm growth occurs at region of low wall shear stress: patient-specific correlation of hemodynamics and growth in a longitudinal study. Stroke 39:2997-3002.
11. Cebral JR, Castro MA, Burgess JE, Pergolizzi RS, Sheridan MJ, et al. (2005) Characterization of cerebral aneurysms for assessing risk of rupture by

using patient-specific computational hemodynamics models. AJNR Am J Neuroradiol 26:2550-2559.

12. Cebral JR, Lohner R (2005) From medical images to computational meshes for CFD. Int J Numer Methods Fluids 47(8-9):985-1008.

13. Cebral JR, Mut F, Sforza D, et al. (2011) Clinical application of image-based CFD for cerebral aneurysms. Int J Numer Method Biomed Eng 27:977-992.

14. Cebral JR, Mut F, Weir J, Putman C (2011) Quantitative characterization of the hemodynamic environment in ruptured and unruptured brain aneurysms. AJNR Am J Neuroradiol 32(1):145-151.

15. Cebral JR, Raschi M. (2013) Suggested connections between risk factors of intracranial aneurysms: a review. Ann Biomed Eng 41:1366-1383.

16. Chen Z, Qin H, Liu J, et al. (2020) Characteristics of wall shear stress and pressure of intracranial atherosclerosis analyzed by a computational fluid dynamics model: a pilot study. Front Neurol 10:1372.

17. Chien A, Tateshima S, Sayre J, Castro M, Cebral J, et al. (2009) Patient-specific hemodynamic analysis of small internal carotid artery-ophthalmic artery aneurysms versus those without blebs. J Neurosurg 111:1235-1241.

18. Chnafa C, Bouillot P, Brina O, et al. (2017) Vessel Calibre and flow splitting relationships at the internal carotid artery terminal bifurcation. Phys Meas 38(11):2044-2057.

19. Chnafa C, Brina O, Pereira V, Steinman D (2018) Better than nothing: a rational approach for minimizing the impact of outflow strategy on cerebrovascular simulations. AJNR Am J Neuroradiol 39(2):337-343.

20. Cho YI, Kensey KR (1991) Effects of the non-newtonian viscosity of blood on flows in a diseased arterial vessel part 1: Steady flows. Biorheology 28(3-4):241-262.

21. Choudhury S, Anupindi K, Patnaik BSV (2021) A study on the transport and interaction between blood flow and low-density-lipoprotein in near-wall regions of blood vessels. Computer Methods Biomech Biomed Eng 24(13):1473-1487.

22. Chung B, Cebral JR. (2015) Cfd for evaluation and treatment planning of aneurysms: review of proposed clinical uses and their challenges. Annals Biomed Eng 43:122-138.

23. Chung BJ, Mut F, Putman CM, Cebral JR. (2014) A comparative study of the hemodynamics of saccular and fusiform aneurysms of the basilar artery. AJNR Am J Neuroradiol 35(6):1163-1169.

24. Connolly ES Jr, Solomon RA (1998) Management of symptomatic and asymptomatic unruptured aneurysms. Neurosurg Clin North America 9(3):509-524.

25. De Santis G, Conti M, Trachet B, De Schryver T, De Beule M, et al. (2013) Haemodynamic impact of stent-vessel (mal)apposition following carotid artery stenting: mind the gaps!. J Biomech 46:908-915.

26. Detmer FJ, Chung BJ, Jimenez C, et al. (2019) Associations of hemodynamics, morphology, and patient characteristics with aneurysm rupture stratified by aneurysm location. Neuroradiology 61:275-284.

27. Dhar S, Tremmel M, Mocco J, et al. (2008) Morphology parameters for intracranial aneurysm rupture risk assessment. Neurosurgery 63(2):185-197.

28. Ergun S (1952) Fluid flow through packed columns. Chem Eng Prog 48(2):89-94.

29. Ergun S, Orning AA (1949) Fluid flow through randomly packed columns and fluidized beds. Ind Eng Chem 41(6):1179-1184.

30. Ettminan N, Beseoglu K, Barrow DL, et al. (2014) Multidisciplinary consensus on assessment of unruptured intracranial aneurysms: proposal of an international research group. Stroke 45:1523-1530.

31. Ford MD, Nikolov HN, Milner JS, et al. (2008) PIV-measured versus CFD-predicted flow dynamics in anatomically realistic cerebral aneurysm models. J Biomech Eng 130:021015.

32. Friedman DP, Maitino AJ (2003) Endovascular interventional neuroradiologic procedures: who is performing them, how often, and where? a survey of academic and nonacademic radiology practices. AJNR Am J Neuroradiol 24(9):1772-1777.

33. Fukazawa K, Ishida F, Umeda Y, et al. (2015) Using computational fluid dynamics analysis to characterize local hemodynamic features of middle cerebral artery aneurysm rupture points. World Neurosurg 83:80-86.

34. Geers AJ, Larrabide I, Radaelli AG, et al. (2014) Reproducibility of image-based computational hemodynamics in intracranial aneurysms: comparison of CTA and 3DRA. Ann Biomed Eng 42:2522-2534.

35. Girfoglio M, Ballarin F, Infantino G, et al. (2022) Non-intrusive podi-rom for patient-specific aortic blood flow in presence of a lvad device. Med Eng Phys 107:103849.

36. Gopalakrishnan SS, Pier B, Biesheuvel A (2014) Dynamics of pulsatile flow through model abdominal aortic aneurysms. J Fluid Mech 758:150-179.

37. Greving JP, Wermer MJ, Brown RD Jr, et al. (2014) Development of the PHASES score for prediction of risk of rupture of intracranial aneurysms: a pooled analysis of six prospective cohort studies. Lancet Neurol 13:59-66.

38. Gundert TJ, Marsden AL, Yang W, LaDisa JF Jr. (2010) Identification of optimal stent design parameters to reduce wall shear stress gradients in coronary arteries. J Biomech Eng 132:091010.

39. Hage ZA, Alaraj A, Arnone GD, Charbel FT (2016) Novel imaging approaches to cerebrovascular disease. Trans Res 175:54-75.

40. Her K, Kim JY, Lim KM, Choi SW. (2018) Windkessel model of hemodynamic state supported by a pulsatile ventricular assist device in premature ventricle contraction. Biomed Eng Online 17:1-13.

41. Himburg HA, Grzybowski DM, Hazel AL, LaMack JA, Li XM, et al. (2004) Spatial comparison between wall shear stress measures and porcine aortic endothelial permeability. Am J Physiol-Heart Circ Physiol 286(5):H1916-H1922.

42. Hodis S, Ding YH, Dai D, et al. (2014) Relationship between aneurysm occlusion and flow diverters: a computational fluid dynamics study. J Neurointerv Surg 6:736-741.

43. Hoi Y, Meng H, Woodward SH, et al. (2004) Effects of arterial geometry on aneurysm growth: three-dimensional computational fluid dynamics study. J Neurosurg 101:676-681.

44. Hope TA, Hope MD, Purcell DD, et al. (2008) Evaluation of intracranial aneurysms with high-resolution 3D quantitative MR angiography: a preliminary study. AJNR Am J Neuroradiol 29:1768-1772.

45. Hoque SZ, Anand DV, Patnaik B (2018) The dynamics of a healthy and infected red blood cell in flow through constricted channels: A dpd simulation. Int J Numer Methods Biomed Eng 34(9):3105.

46. Hoque SZ, Anand DV, Patnaik B (2022) A dissipative particle dynamics simulation of a pair of red blood cells in flow through a symmetric and an asymmetric bifurcated microchannel. Comput Part Mech 9(6):1219-1231.

47. International Study of Unruptured Intracranial Aneurysms Investigators (1998) Unruptured intracranial aneurysms--risk of rupture and risks of surgical intervention. N Engl J Med 339(24):1725-1733.

48. Isoda H, Hirano M, Takeda H, Naganawa S (2010) MR fluid dynamics of the intracranial artery using patient-specific vessel geometry and flow rates. Magn Reson Med Sci 9(4):213-222.

49. Isoda H, Kojima S, Takeda H, et al. (2008) Hemodynamic in a cerebral aneurysm: comparison of magnetic resonance fluid dynamics (MRFD) and computational fluid dynamics (CFD). Neuroradiology 50:904.

50. Isoda H, Naganawa S, Kosugi T (2014) MR fluid dynamics of the intracranial artery: a feasibility study in healthy volunteers. Magn Reson Med Sci 13(4):249.

51. Isoda H, Naganawa S, Kosugi T (2016) Comparison of inflow hemodynamics of intracranial aneurysms between patient-specific CFD and MR fluid dynamics. In: Proc Intl Soc Mag Reson Med. Vol. 24:3426.

52. Isoda H, Naganawa S, Kosugi T (2017) Inflow hemodynamics of intracranial aneurysms: a comparison between patient-specific CFD and MR fluid dynamics. In: Proc Intl Soc Mag Reson Med. Vol. 25:4819.

53. Isoda H, Ohkura Y, Kosugi T, et al. (2010) In vivo hemodynamic analysis of intracranial aneurysms obtained by magnetic resonance fluid dynamics (MRFD) based on time-resolved three-dimensional phase-contrast MRI. Neuroradiology 52:921-928.

54. Isoda H, Ohkura Y, Kosugi T, et al. (2010) Comparison of hemodynamics of intracranial aneurysms between MR fluid dynamics using 3D cine phase-contrast MRI and MR-based computational fluid dynamics. Neuroradiology 52:913-920.

55. Isoda H, Ohno T, Kosugi T, et al. (2010) Comparison of hemodynamics of intracranial aneurysms between MR fluid dynamics using 3D cine phase-contrast MRI and MR-based computational fluid dynamics. Neuroradiology 52:913-920.

56. Isoda H, Hirano M, Takeda H, et al. (2007) Visualization of hemodynamics in intracranial arteries using time-resolved three-dimensional phase-contrast MRI. J Magn Reson Imaging 25:473-478.

57. Jahangiri M, Saghafian M, Sadeghi MR (2017) Numerical simulation of non-newtonian models effect on hemodynamic factors of pulsatile blood flow in elastic stenosed artery. J Mechl Sci Technol 31:1003-1013.

58. Jain K, Jiang J, Strother C, Mardal K A. (2016) Transitional hemodynamics in intracranial aneurysms-comparative velocity investigations with high resolution lattice boltzmann simulations, normal resolution ansys simulations, and mr imaging. Med Phys 43(11):6186

59. Jansen I, Schneiders J, Potters W, et al. (2014) Generalized versus patient-specific inflow boundary conditions in computational fluid dynamics simulations of cerebral aneurysmal hemodynamics. AJNR Am J Neuroradiol 35(8):1543-1548.

60. Jing L, Fan J, He W, Liu X, Li M (2015) Hemodynamic and morphological characteristics of posterior communicating artery aneurysms. J Neurointerv Surg 7(10):771-775.

61. Jou LD, Lee DH, Morsi H, Mawad ME. (2008) Wall shear stress on ruptured and unruptured intracranial aneurysms at the internal carotid artery. AJNR Am J Neuroradiol 29:1761-1767.

62. Juvela S, Korja M. (2017) Intracranial aneurysm parameters for predicting a future subarachnoid hemorrhage: a long-term follow-up study. Neurosurgery 81(3):432-440.

63. Juvela S, Porras M, Poussa K (2000) Natural history of unruptured intracranial aneurysms: a long-term follow-up study. J Neurosurg 93(3):379-387.

64. Juvela S, Poussa K, Lehto H, Porras M (2013) Natural history of unruptured intracranial aneurysms: a long-term follow-up study. Stroke 44:2414-2421.

65. Kaminogo M, Yonekura M, Shibata S (2003) Incidence and outcome of multiple intracranial aneurysms in a defined population. Stroke 34(1):16-21.

66. Kashiwazaki D, Kuroda S. (2013) Size ratio can highly predict rupture risk in intracranial small (<5 mm) aneurysms. Stroke 44:2169-2173.

67. Kassell NF, Torner JC, Haley EC, Jane JA, Adams HP, et al. (1990) The international cooperative studyon the timing of aneurysm surgery: Part 1: Overall management results. J Neurosurg 73(1):18-36.

68. Khan MO, Valen-Sendstad K, Steinman DA. (2015) Narrowing the expertise gap for predicting intracranial aneurysm hemodynamics: impact of solver numerics vs. mesh and time-step resolution. AJNR Am J Neuroradiol 36:1310-1316.

69. King JT, Berlin JA, Flamm ES. (1994) Morbidity and mortality from elective surgery for asymptomatic, unruptured, intracranial aneurysms: a meta-analysis. J Neurosurg 81(6):837-842.

70. Kojima S, Isoda H, Hirano M, et al. (2014) A practical method for confirming hemodynamic flow in cerebral aneurysms by using MR fluid dynamics. Magn Reson Med Sci 13:199-203.

71. Kono K, Fujimoto T, Shintani A, Terada T (2012) Hemodynamic characteristics at the rupture site of cerebral aneurysms: a case study. Neurosurgery 71: ONS120-ONS129; discussion ONS129.

72. Kono K, Terada T (2013) Hemodynamics of the anterior communicating artery: a computational fluid dynamics study. Neurol Res 35:845-852.

73. Krings T, Hans F-J, Geibprasert S, Terbrugge K (2010) Partial "targeted" Embolisation of brain arteriovenous malformations. Eur Radiol 20:2723-2731.

74. Ku DN, Giddens DP, Zarins CK, Glagov S (1985) Pulsatile flow and atherosclerosis in the human carotid bifurcation. Positive correlation between plaque location and low and oscillating shear stress. Arteriosclerosis 5(3):293-302.

75. Kumar D, Vinoth R, Raviraj A, Shankar CV (2017) Non-newtonian and newtonian blood flow in human aorta: a transient analysis. Biomed Res (India) 28(7):3194-3203.

76. Laurie A, Baharoglu MI, Malek AM. (2012) Ruptured status discrimination performance of aspect ratio, height/width, and bottleneck factor is highly dependent on aneurysm sizing methodology. Neurosurgery 71:38-45; discussion 45-46.

77. Le Roux PD, Winn HR (1998) Management of the ruptured aneurysm. Neurosurg Clin North America 9(3):525-540.

78. Lei H, Caswell B, Karniadakis GE (2010) Direct construction of mesoscopic models from microscopic simulations. Phys Rev E 81(2):026704.

79. Leng X, Scalzo F, Ip HL, et al. (2014) Computational fluid dynamics modeling of symptomatic intracranial atherosclerosis may predict risk of stroke recurrence. PLoS One 9(5):97531.

80. Li J, Jin M, Sun X, et al. (2019) Imaging of Moyamoya disease and Moyamoya syndrome: current status. J Comput Assist Tomograph 43(2):257.

81. Liang L, Steinman DA, Brina O, Chnafa C, Cancel M, et al. (2015) A novel approach for quantitative analysis of intra-aneurysmal hemodynamics: towards the prediction of rupture risk. J Biomech 48:3135-3140.

82. Lin N, Ho A, Charoenvimolphan N, Frerichs KU, Day AL, et al. (2013) Analysis of morphological parameters to differentiate rupture status in anterior communicating artery aneurysms. PLoS One 8(11):79635.

83. Lin N, Ho A, Gross BA, et al. (2012) Differences in simple morphological variables in ruptured and unruptured middle cerebral artery aneurysms. J Neurosurg 117(5):913-919.

84. Liu H, Lan L, Abrigo J, et al. (2021) Comparison of newtonian and non-newtonian fluid models in blood flow simulation in patients with intracranial arterial stenosis. Front Physiol 12:718540.

85. Lu G, Huang L, Zhang XL, et al. (2011) Influence of hemodynamic factors on rupture of intracranial aneurysms: patient-specific 3D mirror aneurysms model computational fluid dynamics analysis. AJNR Am J Neuroradiol 32:1255-1261.

86. Mahalingam A, Gawandalkar UU, Kini G, et al. (2016) Numerical analysis of the effect of turbulence transition on the hemodynamic parameters in human coronary arteries. Cardiovas Diagn ther 6(3):208.

87. Malek AM, Alper SL, Izumo S (1999) Hemodynamic shear stress and its role in atherosclerosis. JAMA 282(21):2035-2042.

88. Maramkandam EB, Sudhir BJ, Kannath SK, Patnaik BSV (2023) A novel parameter for the prediction of rupture risk of cerebral aneurysms based on morphology. Proc Institut Mech Eng Part H J Eng Med 9:1091-1101.

89. Markl M, Frydrychowicz A, Kozerke S, Hope M, Wieben O (2012) 4D flow MRI. J Magn Reson Imaging 36(5):1015-1036.

90. Meckel S, Stalder AF, Santini F, et al. (2008) In vivo visualization and analysis of 3D hemodynamics in cerebral aneurysms with flow-sensitized 4D MR imaging at 3T. Neuroradiology 50:473-484.

91. Meng H, Tutino VM, Xiang J, Siddiqui A (2014) High WSS or low WSS? Complex interactions of hemodynamics with intracranial aneurysm initiation, growth, and rupture: toward a unifying hypothesis. AJNR Am J Neuroradiol 35(7):1254-1262.

92. Meng H, Wang Z, Hoi Y, et al. (2007) Complex hemodynamics at the apex of an arterial bifurcation induces vascular remodeling resembling cerebral aneurysm initiation. Stroke 38:1924-1931.

93. Miura Y, Ishida F, Umeda Y, et al. (2013) Low wall shear stress is independently associated with the rupture status of middle cerebral artery aneurysms. Stroke 44:519-521.

94. Morita A, Kirino T, Hashi K, et al. (2012) The natural course of unruptured cerebral aneurysms in a Japanese cohort. N Engl J Med 366:2474-2482.

95. Nader E, Skinner S, Romana M, et al. (2019) Blood rheology: key parameters, impact on blood flow, role in sickle cell disease and effects of exercise. Front Physiol 10:1329.

96. Nagargoje M, Gupta R (2020) Effect of sinus size and position on hemodynamics during pulsatile flow in a carotid artery bifurcation. Computer Methods Prog Biomed 192:105440.

97. Nagargoje MS, Mishra DK, Gupta R (2021) Pulsatile flow dynamics in symmetric and asymmetric bifurcating vessels. Phys Fluids 33(7): 071904

98. Naito T, Miyachi S, Matsubara N, et al. (2012) Magnetic resonance fluid dynamics for intracranial aneurysms: comparison with computed fluid dynamics. Acta Neurochir (Wien) 154:993-1001.

99. Nett EJ, Johnson KM, Frydrychowicz A, et al. (2012) Four-dimensional phase contrast MRI with accelerated dual velocity encoding. J Magn Reson Imaging 35:1462-1471.

100. Nieuwkamp DJ, Setz LE, Algra A, Linn FH, de Rooij NK, et al. (2009) Changes in case fatality of aneurysmal subarachnoid haemorrhage over time, according to age, sex, and country: a meta-analysis. Lancet Neurol 8(7):635-642.

101. Nordahl ER, Uthamaraj S, Dennis KD, et al. (2021) Morphological and hemodynamic changes during cerebral aneurysm growth. Brain Sci 11(4):520.

102. Omodaka S, Sugiyama S, Inoue T, et al. (2012) Local hemodynamics at the rupture point of cerebral aneurysms determined by computational fluid dynamics analysis. Cerebrovasc Dis 34:121-129.

103. Patel S, Usmani AY, Muralidhar K (2017) Effect of aorto-iliac bifurcation and iliac stenosis on flow dynamics in an abdominal aortic aneurysm. Fluid Dynam Res 49(3):035513.

104. Pereira VM, Brina O, Bijlenga P, et al. (2013) Wall shear stress distribution in a patient-specific intracranial aneurysm model: comparison of conventional and high-resolution 3D rotational angiography. J Neurointerv Surg 5:288-293.

105. Philip NT, Bolem S, Sudhir BJ, Patnaik BSV (2022) Hemodynamics and bio-mechanics of morphologically distinct saccular intracranial aneurysms at bifurcations: Idealised vs patient-specific geometries. Computer Methods Prog Biomed 227:107237.

106. Prell D, Kyriakou Y, Struffert T, Dörfler A, Kalender W (2010) Metal artifact reduction for clipping and coiling in interventional c-arm ct. AJNR Am J Neuroradiol 31(4):634-639.

107. Qian Y, Takao H, Umezu M, Murayama Y. (2011) Risk analysis of unruptured aneurysms using computational fluid dynamics technology: preliminary results. AJNR Am J Neuroradiol 32:1948-1955.

108. Raaymakers TWM, Rinkel GJE, Limburg M, Algra A. (1998) Mortality and morbidity of surgery for unruptured intracranial aneurysms: a meta-analysis. Stroke 29(8):1531-1538.

109. Raghavan ML, Ma B, Harbaugh RE (2005) Quantified aneurysm shape and rupture risk. J Neurosurg 102(2):355-362.

110. Raschi M, Mut F, Byrne G, et al. (2012) CFD and PIV analysis of hemodynamics in a growing intracranial aneurysm. Int J Numer Method Biomed Eng 28:856-868.

111. Rayz VL, Boussel L, Acevedo-Bolton G, et al. (2008) Numerical simulations of flow in cerebral aneurysms: comparison of CFD results and in vivo MRI measurements. J Biomech Eng 130:051011.

112. Ren Y, Chen GZ, Liu Z, Cai Y, Lu GM, et al. (2017) Reproducibility of image-based computational models of intracranial aneurysm: a comparison between 3D rotational angiography and CT angiography. Acta Neurochir (Wien) 159:1909-1919.

113. Rinkel GJ, Algra A (2011) Long-term outcomes of patients with aneurysmal subarachnoid haemorrhage. Lancet Neurol 10:349-350.

114. Rinkel GJ, Djibuti M, Algra A, van Gijn J (1998) Prevalence and risk of rupture of intracranial aneurysms: a systematic review. Stroke 29(1):251-256.

115. Rutkowski DR, Roldán-Alzate A, Johnson KM (2021) Enhancement of cerebrovascular 4d flow mri velocity fields using machine learning and computational fluid dynamics simulation data. Scient Rep 11(1):10240.

116. Saxena A, Ng EYK, Lim ST. (2019) Imaging modalities to diagnose carotid artery stenosis: progress and prospect. Biomed Eng Online 18:1-23.

117. Sazonov I, Nithiarasu P (2012) Semi-automatic surface and volume mesh generation for subject-specific biomedical geometries. Int J Numer Methods Biomed Eng 28(1):133-157.

118. Schievink WI (1997) Intracranial aneurysms. N Engl J Med. 1997 336(1):28-40.

119. Schneiders JJ, Marquering HA, van Ooij P, et al. (2015) Additional value of intra-aneurysmal hemodynamics in discriminating ruptured versus unruptured intracranial aneurysms. AJNR Am J Neuroradiol 36:1920-1926.

120. Schnell S, Ansari SA, Vakil P, et al (2014) Three-dimensional hemodynamics in intracranial aneurysms: influence of size and morphology. J Magn Reson Imaging 39:120-131.

121. Seymour RS, Hu Q, Snelling EP (2020) Blood flow rate and wall shear stress in seven major cephalic arteries of humans. J Anatomy 236(3):522-530.

1.

122. Sforza DM, Putman CM, Cebral JR (2009) Hemodynamics of cerebral aneurysms. Annual Rev Fluid Mech 41:91-107.

123. Sforza DM, Putman CM, Tateshima S, Viñuela F, Cebral JR (2012) Effects of perianeurysmal environment during the growth of cerebral aneurysms: a case study. AJNR Am J Neuroradiol 33:1115-1120.

124. Shimogonya Y, Ishikawa T, Imai Y, Yamaguchi T. (2009) Can the pressure loss coefficient be an indicator for the rupture risk of cerebral aneurysms? J Biomech 42(4):548-551.

125. Sho E, Sho M, Hoshina K, Kimura H, Nakahashi TK, et al (2004) Hemodynamic forces regulate mural macrophage infiltration in experimental aortic aneurysms. Exp Mol Pathol 76:108-116.

126. Shojima M, Oshima M, Takagi K, et al. (2004) Magnitude and role of wall shear stress on cerebral aneurysm: computational fluid dynamic study of 20 middle cerebral artery aneurysms. Stroke 35:2500-2505.

127. Singla R, Gupta S, Chanda A. (2023) A computational fluid dynamics-based model for assessing rupture risk in cerebral arteries with varying aneurysm sizes. Math Computl Appl 28(4):90.

128. Sinnaswamy RA, Palanisamy N, Subramaniam K, Muthusamy S, Lamba R, et al. (2023) An extensive review on deep learning and machine learning intervention in prediction and classification of types of aneurysms. Wireless Personal Commun 1-26.

129. Skodvin TØ, Johnsen L-H, Gjertsen Ø, Isaksen JG, Sorteberg A (2017) Cerebral aneurysm morphology before and after rupture: nationwide case series of 29 aneurysms. Stroke 48(4):880-886.

130. Skodvin TØ, Johnsen LH, Gjertsen Ø, Isaksen JG, Sætran LR. (2017) Aneurysm rupture and the association with smoking. A case-control study. Acta Neurochir 159(1):55-61.

131. Solomon RA, Fink ME, Pile-Spellman J (1994) Surgical management of unruptured intracranial aneurysms. J Neurosurg 80(3):440-446.

132. Sonobe M, Yamazaki T, Yonekura M, Kikuchi H (2010) Small unruptured intracranial aneurysm verification study: SUAVe study, Japan. Stroke 41:1969-1977.

133. Steinman DA, Hoi Y, Fahy P, et al. (2013) Variability of computational fluid dynamics solutions for pressure and flow in a giant aneurysm: the ASME 2012 Summer Bioengineering Conference CFD Challenge. J Biomech Eng 135:021016.

134. Steinman DA, Milner JS, Norley CJ, Lownie SP, Holdsworth DW (2003) Image-based computational simulation of flow dynamics in a giant intracranial aneurysm. AJNR Am J Neuroradiol 24:559-566.

135. Steinman DA, Pereira VM (2019) How patient specific are patient-specific computational models of cerebral aneurysms? an overview of sources of error and variability. Neurosurg Focus 47(1):14.

136. Steinman DA, Taylor CA (2005) Flow imaging and computing: a new era in the study of hemodynamics. Circulation 111(21):2742-2744.

137. Sugiyama S, Endo H, Omodaka S, et al. (2017) Wall shear stress, flow pulsatility, and temporal shear gradient in unruptured intracranial aneurysms. J Neuroendovascular Ther 11:371-378.

138. Sugiyama S, Meng H, Funamoto K, et al. (2017) Hemodynamic analysis of growing intracranial aneurysms arising from a posterior inferior cerebellar artery. World Neurosurg 97:364-372.

139. Sugiyama S, Niizuma K, Nakayama T, et al. (2013) Relative residence time prolongation in intracranial aneurysms: a possible association with atherosclerosis. Neurosurgery 73:767-776.

140. Sugiyama SI, Niizuma K, Nakayama T, Shimizu H, Endo H, et al. (2013) Relative residence time of micro-catheter is a risk factor for thrombus formation in intracranial aneurysm embolization. Stroke 44(11):3278-3280.

141. Suh G-Y, Les AS, Tenforde AS, et al. (2011) Hemodynamic changes quantified in abdominal aortic aneurysms with increasing exercise intensity using mr exercise imaging and image-based computational fluid dynamics. Annals Biomed Eng 39:2186-2202.

142. Takao H, Murayama Y, Otsuka S, et al. (2012) Hemodynamic differences between unruptured and ruptured intracranial aneurysms during observation. Stroke 43:1436-1439.

143. Takehara Y, Isoda H, Takahashi M, et al. (2017) Accuracy of 4D flow MRI for measurements of WSS in cerebral aneurysms: a reproducibility study. Magn Reson Med Sci 16:345-346.

144. Taylor CA, Figueroa C (2009) Patient-specific modeling of cardiovascular mechanics. Annual Rev Biomed Eng 11:109-134.

145. Thomas HJ, Rana U, Marsh CE, et al. (2020) Assessment of cerebrovascular responses to physiological stimuli in identical twins using multimodal imaging and computational fluid dynamics. J Appl Physiol 129(5):1024-1032.

146. Ujiie H, Tachibana H, Hiramatsu O, et al. (1999) Effects of size and shape (aspect ratio) on the hemodynamics of saccular aneurysms: a possible index for surgical treatment of intracranial aneurysms. Neurosurgery 45:119-129; discussion 129-130.

147. Ujiie H, Tamano Y, Sasaki K, Hori T (2001) Is the aspect ratio a reliable index for predicting the rupture of a saccular aneurysm? Neurosurgery 48(3):495-503.

148. Unruptured Intracranial Aneurysms Investigators IS. (1998) Unruptured intracranial aneurysms-risk of rupture and risks of surgical intervention. N Engl J Med 339(24):1725-1733.

149. Usmani AY, Muralidhar K (2021) Unsteady hemodynamics in intracranial aneurysms with varying dome orientations. J Fluids Eng 143(6): 061206.

150. Valen-Sendstad K, Bergersen AW, Shimogonya Y, et al. (2018) Real-world variability in the prediction of intracranial aneurysm wall shear stress: the 2015 international aneurysm cfd challenge. Cardiovascular Eng Technol 9:544-564.

151. Valen-Sendstad K, Piccinelli M, KrishnankuttyRema R, Steinman DA (2014) Estimation of turbulent wall shear stress in a subject-specific intracranial aneurysm. J Biomech 47:2756-2762.

152. Valen-Sendstad K, Steinman DA (2014) Mind the gap: impact of computational fluid dynamics solution strategy on prediction of intracranial aneurysm hemodynamics and rupture status indicators. AJNR Am J Neuroradiol 35(3):536-543.

153. Valencia AA, Guzman AM, Finol EA, Amon CH (2006) Blood flow dynamics in saccular aneurysm models of the basilar artery. J Biomech Eng 128:516-526.

154. van Gijn J, Rinkel GJ (2001) Subarachnoid haemorrhage: diagnosis, causes and management. Brain 124(2):249-278.

155. van Ooij P, Potters WV, Collins J, et al. (2015) Characterization of abnormal wall shear stress in patients with bicuspid aortic valve disease using 4D flow MRI. Magn Reson Med 73(5):1749-1761.

156. van Ooij P, Potters WV, Guédon A, et al. (2013) Wall shear stress estimated with phase contrast MRI in an in vitro and in vivo intracranial aneurysm. J Magn Reson Imaging 38:109-116.

157. van Ooij P, Potters WV, Nederveen AJ, et al. (2015) A methodology to detect abnormal relative wall shear stress on the full surface of the thoracic aorta using four-dimensional flow MRI. Magn Reson Med 73:1216-1227.

158. Varble N, Tutino VM, Yu J, et al. (2018) Shared and distinct rupture discriminants of small and large intracranial aneurysms. Stroke 49(4):856-864.

159. Vernooij MW, Ikram MA, Tanghe HL, et al. (2007) Incidental findings on brain MRI in the general population. N Engl J Med 357:1821-1828.

160. Vignon-Clementel IE, Figueroa CA, Jansen KE, Taylor CA (2006) Outflow boundary conditions for three-dimensional finite element modeling of blood flow and pressure in arteries. Comput Methods Appl Mech Eng 195(29-32):3776-3796.

161. Vlak MH, Algra A, Brandenburg R, Rinkel GJ (2011) Prevalence of unruptured intracranial aneurysms, with emphasis on sex, age, comorbidity, country, and time period: a systematic review and meta-analysis. Lancet Neurol 10(7):626-636.

162. Walburn FJ, Schneck DJ (1976) A constitutive equation for whole human blood. Biorheology 13(3):201-210.

163. Wang L, Wang L-P, Guo Z, Mi J. (2015) Volume-averaged macroscopic equation for fluid flow in moving porous media. Int J Heat Mass Transfer 82:357-368.

164. Weir B (2002) Unruptured intracranial aneurysms: a review. J Neurosurg 96(1):3-42.

165. Wei Z, Singh-Gryzbon S, Trusty PM, et al. (2020) Non-newtonian effects on patient-specific modeling of fontan hemodynamics. Annals Biomed Eng 48:2204-2217.

166. Whitaker S (1986) Flow in porous media 1: a theoretical derivation of Darcy's law. Transport Porous Media 1:3-25.

167. Wiebers DO (2003) Unruptured intracranial aneurysms: natural history, clinical outcome, and risks of surgical and endovascular treatment. Lancet 362(9378):103-110.

168. Wiebers DO, Piepgras DG, Meyer FB, et al. (2004) Pathogenesis, natural history, and treatment of unruptured intracranial aneurysms. Mayo Clinic Proc 79:1572-1583.

169. Xiang J, Natarajan SK, Tremmel M, et al. (2011) Hemodynamic-morphologic discriminants for intracranial aneurysm rupture. Stroke 42(1):144-152.

170. Xiang J, Siddiqui AH, Meng H, Kolega J (2014) The role of complex hemodynamics in the localization of intracranial aneurysm initiation. J Biomech 47(1):89-95.

171. Yamashita S, Isoda H, Hirano M, et al. (2007) Visualization of hemodynamics in intracranial arteries using time-resolved three-dimensional phase-contrast MRI: clinical applications. Neuroradiology 49(suppl 1): S93-S94.

172. Zhang Y, Mu S, Chen J, et al. (2016) Hemodynamic analysis of intracranial aneurysms with daughter blebs. J Neurointerv Surg 8:828-833.

173. J Xi, K. Barari, X Si, MYA Jamalabadi, J Park, et al. (2022) Inspiratory Leakage Flow Fraction for Surgical Masks with Varying Gaps and Filter Materials. Physics of Fluids, 34: 041902.

174. R Sadeghi, M Shadloo, MYA Jamalabadi, A Karimipour (2016) A three-dimensional lattice Boltzmann model for numerical investigation of bubble growth in pool boiling, International Communications in Heat and Mass Transfer, 79: 58- 66.

175. A Shahidian, M Ghassemi, S Khorasanizade, MYA Jamalabadi, G Ahmadi (2009) Flow Analysis of Non- Newtonian Blood in a Magnetohydrodynamic Pump. IEEE Transactions on Magnetics 45 (6): 2667- 2670.

176. MYA Jamalabadi, J Xi (2022) Olfactory Drug Aerosol Delivery with Acoustic Radiation. Biomedicine, 10:1347.

177. MYA Jamalabadi, M Shirazi, H Nasiri, MR Safaei, TK Nguyen (2018) Modeling and analysis of biomagnetic Blood Carreau fluid flow through a stenosed artery with magnetic heat transfer; a transient study. PLoS ONE, 13(2): e0192138.

178. MYA Jamalabadi, A Bidokhti, H Rah, S Vaezi, P (2016) Hooshmand Numerical Investigation of Oxygenated and Deoxygenated Blood Flow through a Tapered Stenosed Arteries in Magnetic Field. PLoS ONE 11(12): e0167393. 1-23.

179. MYA Abdollahzadeh Jamalabadi, P Hooshmand, A Hesabi, M K Kwak, et al. (2016) Numerical Investigation of Thermal Radiation and Viscous effects on Entropy Generation in Forced Convection Blood Flow over Axisymmetric Stretching Sheet. entropy, 18 (6): 203-218.

180. S Bita, MYA Jamalabadi, M Mesbah (2015) Toxicity study of silver nanoparticles synthesized using seaweed Sargassum angustifolium in common carp, Cyprinus carpio. Journal of Chemical and Pharmaceutical Research 7(11): 91-98.

181. MYA Jamalabadi, S Dousti (2015) Feasibility study of magnetic effects on silver nanoparticles for drug and gene delivery in Cyprinus carpio. Journal of Chemical and Pharmaceutical Research 7(12): 206-218.

182. MYA Jamalabadi (2016) Microrobots Propulsion system design for drug delivery. Journal of Chemical and Pharmaceutical Research 8 (2): 448-469.

183. MYA Jamalabadi, A Keikha (2016) Fluid- Solid interaction modeling of Cerebrospinal fluid absorption in arachnoid villi. Journal of Chemical and Pharmaceutical Research 8 (2): 428-442.

184. A Keikha, MYA Jamalabadi (2016) Optimal design of magnetic field for reaction control in drug delivery applications. Journal of Chemical and Pharmaceutical Research 8(5): 420-428.

185. A Keikha, MYA Jamalabadi (2016) Numerical viscous heating effects in renal artery stenosis under peristaltic wall motions. Journal of Chemical and Pharmaceutical Research 8(5): 689-706.

186. S Bita, A Keikha, MYA Jamalabadi (2016) Toxicity study of silver nanoparticles synthesized using aqueous and alcoholic extract of seaweed Sargassum angustifolium in Barbus sharpeyi. Journal of Chemical and Pharmaceutical Research 8(5): 707-712.

187. MYA Jamalabadi (2021) Use of Nanoparticle Enhanced Phase Change Material for Cooling of Surface Acoustic Wave Sensor. fluids 6(31): 710-805.

188. P Hooshmand, MYA Jamalabadi, H K Balotaki (2016) MHD effects on magnetic silver nanoparticles oxidative stress and apoptosis in Cyprinus carpio. International Journal of Pharmaceutical Research and Allied Sciences 5(2): 293-304.

189. MYA Jamalabadi, A Keikha (2016) Numerical investigation of Magneto hydrodynamics effects on natural silver nanoparticles from Sargassum angustifolium used for transporting a pharmaceutical compound in Cyprinus carpio. Entomology and Applied Science Letters 3(2): 52-64.

190. MYA Jamalabadi (2016) Energy harvesting by micro-turbine in blood arteries for bio applications. International Journal of Pharmaceutical Research and Allied Sciences 5(3): 52-74.

191. MYA Jamalabadi, M Shirazi, A Kosar, M Shadloo (2017) Effect of injection angle, density ratio, and viscosity on droplet formation in a microfluidic t-junction. Theoretical and Applied Mechanics Letters 7(4): Pp 243-251.

192. MYA Jamalabadi (2026) A Molecular Key to the Filter: Podocin Phosphorylation Unveiled in a Case of Early-Stage Steroid-Resistant Nephrotic Syndrome. Annals of Clinical and Medical Case Reports 15(1): 1-11.

193. MYA Jamalabadi (2025) A Conservative Numerical Framework for Modeling Nonlinear Ultrasound Propagation in Thermo-viscous Tissue Phantom, Mathews Journal of Surgery 8(2): 41: Pp 1-11.

194. MYA Jamalabadi (2025) A Comprehensive Review of Computational Modeling in Tumor and Brain Disorder with a Focus on Ablation Therapies. Journal of Biomedical Research Environmental Sciences 6(10): 19-35.

195. MYA Jamalabadi (2025) Cracking the Molecular Matrix: Next-Gen AI Reshapes Biomedicine. World Journal of Pharmaceutical and Healthcare Research 2(8): 19-35.

196. MYA Jamalabadi (2025) Smart Lubrication for Joints: Carbon Nanomaterials in Biomedical Applications. Journal of Applied Mechanics Reviews and Reports 1(1): 1-13.

197. MYA Jamalabadi (2025) A Comprehensive Review on Deep Learning for Genomics and AI in Drug Discovery. Available at Preprints

198. MYA Jamalabadi (2025) Superiority of Carbon Nanocomposites on Diarthrosis Lubrication. New Energy Exploitation.

199. A Hosseinian, MYA Jamalabadi (2024) Numerical Investigation of Temperature Field in Hyperthermia Considering Diffusion in Interstitial Tissue. Available at SSRN 4786896

200. MYA Jamalabadi (2022) Electrohydrodynamic Squeeze- Film Interaction in Synovial Joints. Recent Progress in Materials 4: 1- 21.

201. MYA Jamalabadi (2022) Parameter study of the J- integral over a craze line in a root canalled tooth, Medical Research and Innovations 6: 1- 5.

202. MYA Jamalabadi (2022) Numerical modeling of olfactory drug delivery with acoustic streaming. Ankara international congress on scientific research-VI April Pp: 536-544.

203. MYA Jamalabadi (2021) Pool boiling of oscillating magnetic cylinder with LBM. 7th INTERNATIONAL MARDIN ARTUKLU SCIENTIFIC RESEARCHES CONFERENCE December Pp: 10-12.